

## Flux motion, proximity effect, and critical current density in $\text{YBa}_2\text{Cu}_3\text{O}_{7-\delta}$ /silver composites

J. Jung, M. A.-K. Mohamed, S. C. Cheng, and J. P. Franck

*Department of Physics, University of Alberta, Edmonton, Alberta, Canada T6G 2J1*

(Received 1 March 1990; revised manuscript received 18 June 1990)

We report on studies of magnetic and transport properties, as well as on characterization of defects in the pure  $\text{YBa}_2\text{Cu}_3\text{O}_{7-\delta}$  and the  $\text{YBa}_2\text{Cu}_3\text{O}_{7-\delta}/\text{Ag}$  (10 and 30 wt. %) composites. The studies of magnetic properties include the diamagnetic shielding, the Meissner effect, the trapped field [for both zero-field-cooling (ZFC) and field-cooling (FC) cases], and their dependence on applied magnetic field, temperature, and time. High- and low-magnetic-field hysteresis loops were measured and the intragrain "magnetic" critical current density was calculated. The studies of transport properties include the resistivity and intergrain "transport" critical-current-density measurements. Distribution, spacing, and size of intragrain twin boundaries were investigated. The results show the degradation of superconducting properties if silver is added to  $\text{YBa}_2\text{Cu}_3\text{O}_{7-\delta}$  during the sintering process, except the enhancement of the intergrain critical current density  $J_{\text{CT}}$  in  $\text{YBa}_2\text{Cu}_3\text{O}_{7-\delta}/\text{Ag}$  (10 wt. %) composite. The activation energy for intergranular flux creep of 1.6 and  $\sim 0.3$  eV was found for the pure  $\text{YBa}_2\text{Cu}_3\text{O}_{7-\delta}$  and the  $\text{YBa}_2\text{Cu}_3\text{O}_{7-\delta}/\text{Ag}$  composites, respectively. The results did not show any relationship between  $J_{\text{CT}}$ , the activation energy, and the number of pinning centers (the trapped field) in these samples. It is suggested that the proximity junctions superconductor-normal-metal-superconductor built up by intergranular silver, and not flux pinning, are responsible for the increase of  $J_{\text{CT}}$ . Defect characterization by transmission electron microscopy revealed that silver does not affect the structure of twin boundaries inside the grains of  $\text{YBa}_2\text{Cu}_3\text{O}_{7-\delta}$ .

### I. INTRODUCTION

There have been intensive studies of silver-doped high-temperature ceramic superconductors during the past two years. These studies were motivated by the hypothesis that the intergrain resistance that limits high critical currents could be reduced by the presence of silver in the intergranular space of the ceramic sample. It was reported that doping with silver enhances critical currents of intergrain contacts (weak links) in  $\text{YBa}_2\text{Cu}_3\text{O}_{7-\delta}$  usually by a factor of 2–3 measured at 77 K and zero applied magnetic field for a silver substitution level over a range of 3–30 wt. %.<sup>1–7</sup> A large increase of the "transport" critical current density in  $\text{YBa}_2\text{Cu}_3\text{O}_{7-\delta}/\text{Ag}$  composites by 1 and 2 orders of magnitude was also reported.<sup>8–10</sup> Silver was found to degrade the superconducting properties of  $\text{YBa}_2\text{Cu}_3\text{O}_{7-\delta}$  if substituted for copper.<sup>11</sup>  $\text{YBa}_2(\text{Cu}_{1-x}\text{Ag}_x)_3\text{O}_{7-\delta}$  exists as a single-phase material for only  $x \leq 0.1$ . Silver added to  $\text{YBa}_2\text{Cu}_3\text{O}_{7-\delta}$  before the sintering process, in a form of metal or oxide powder, resides in the intergranular space of the ceramic sample, filling voids and coating  $\text{YBa}_2\text{Cu}_3\text{O}_{7-\delta}$  grain boundaries.<sup>2,6,12–15</sup> During the sintering process silver cleans the surface of  $\text{YBa}_2\text{Cu}_3\text{O}_{7-\delta}$  grains by chemical reaction with compounds existing at the grain surface (e.g.,  $\text{BaCuO}_2$ ,  $\text{BaCO}_3$ ) (Ref. 16) and does not diffuse into the  $\text{YBa}_2\text{Cu}_3\text{O}_{7-\delta}$  phase.<sup>16</sup> The interfaces between  $\text{YBa}_2\text{Cu}_3\text{O}_{7-\delta}$  and silver were found to be nonreactive.<sup>17</sup>

The factors listed above are responsible for the improved coupling between superconducting grains (the re-

duced contact resistance between grains). Silver causes significant grain growth through partial melting of  $\text{YBa}_2\text{Cu}_3\text{O}_{7-\delta}$  (Refs. 18 and 19) and creates a uniform grain size distribution with a mean grain size of  $15 \mu\text{m}$ ,<sup>6</sup> while pure  $\text{YBa}_2\text{Cu}_3\text{O}_{7-\delta}$  usually displays a broad distribution of grain size.

The suspension of a sample of  $\text{YBa}_2\text{Cu}_3\text{O}_{7-\delta}/\text{Ag}$  composite, while superconducting, beneath a magnet was first observed by Peters *et al.*<sup>10</sup> This effect was believed to be due to strong pinning forces provided by higher intergranular critical currents. The presence of strong pinning forces in  $\text{YBa}_2\text{Cu}_3\text{O}_{7-\delta}/\text{Ag}$  composites has been later proved by Shapira *et al.*<sup>20</sup> A large remanent moment was inferred from magnetic hysteresis loop measurements up to 1.2 kG at 4.2 and 77 K. However, Jin *et al.*<sup>21</sup> have argued that the suspension behavior observed in  $\text{YBa}_2\text{Cu}_3\text{O}_{7-\delta}/\text{Ag}$  composites is a consequence of large grain size and not due to the presence of AgO or Ag particles. There appears to be no substantial enhancement of flux pinning and "magnetic" critical current density [calculated from high-field (15 kG) magnetization hysteresis loops at 77 K] by these particles. The pinning force and hence the "magnetic" critical current density of melt-textured pure  $\text{YBa}_2\text{Cu}_3\text{O}_{7-\delta}$  superconductor turns out to be a factor of 2 larger [ $J_{\text{CM}}(\text{magn.}) \sim 10^4$  A/cm<sup>2</sup> at 77 K] than those of  $\text{YBa}_2\text{Cu}_3\text{O}_{7-\delta}/\text{Ag}$  ceramic composites. Studies done by Pavuna *et al.*<sup>14</sup> and Dwir *et al.*<sup>2</sup> on  $\text{YBa}_2\text{Cu}_3\text{O}_{7-\delta}/\text{Ag}$  (9.1 wt. %) composite revealed that intragranular  $J_{\text{CM}}$  estimated from high-field (18 T) hysteresis loops (to be about  $10^5$  A/cm<sup>2</sup> at 4.2 K) is not

strongly affected (maximum increase  $\sim 15\%$ ) by intergranular silver.

The role of intergranular silver in enhancing the critical "transport" current density of  $\text{YBa}_2\text{Cu}_3\text{O}_{7-\delta}/\text{Ag}$  composites has not been clear. Two effects have been suggested: a higher activation energy for intergranular flux motion induced by the presence of silver or improved coupling between silver-coated superconducting grains due to proximity-induced coherence length. The first possibility has been analyzed by Ma *et al.*<sup>22</sup> on the basis of the measurements of the angular dependence of magnetization (at 77 K and  $H=20$  G) and low-field (40 G) hysteresis loops at 77 K of  $\text{YBa}_2\text{Cu}_3\text{O}_{7-\delta}/\text{Ag}$  composites, concluding that Ag doping strengthens the flux pinning. The energy of a pinning center was calculated to be about 0.3 eV for the  $\text{YBa}_2\text{Cu}_3\text{O}_{7-\delta}/\text{Ag}$  (5, 15, and 30 wt. %) composites and 0.2 eV for the pure  $\text{YBa}_2\text{Cu}_3\text{O}_{7-\delta}$  sample at 77 K. The second effect has been suggested by Weinberger *et al.*<sup>6</sup> and Miller *et al.*<sup>12</sup>

In this paper we present measurements of magnetic properties of the pure  $\text{YBa}_2\text{Cu}_3\text{O}_{7-\delta}$  ceramics and the  $\text{YBa}_2\text{Cu}_3\text{O}_{7-\delta}/\text{Ag}$  (10 and 30 wt. %) ceramic composites. The measurement of the spatial distributions of the magnetic field across disk-shaped samples both for the zero-field-cooling and field-cooling cases, provided the information on the flux expulsion, penetration, and pinning at 77 K over an applied magnetic field range 0–1200 G. The activation energy for intergranular flux creep has been calculated from the dependence of the trapped magnetic field on time. The magnitude of the remanent magnetic moment has been inferred from the measurements of dc magnetization as a function of temperature and applied magnetic field. The intragranular (magnetic) critical current densities have been calculated from the high- (45 kG) magnetic-field hysteresis loops measured at 77 and 10 K. The intergranular (transport) critical current densities have been measured at 77 K and  $H \leq 0.5$  G (the Earth magnetic field). The sample characterization also included resistivity and low-field (10 G) dc magnetization measurements to determine superconducting transition temperatures; scanning electron microscopy (SEM) and transmission electron microscopy (TEM) to analyze the distribution of grain sizes, silver inclusions, and the presence of twin boundaries inside the grains of  $\text{YBa}_2\text{Cu}_3\text{O}_{7-\delta}/\text{Ag}$  composites, and x-ray powder diffraction to analyze changes in the lattice constants.

The results of this work suggest that the proximity junctions and not flux pinning are responsible for the silver-enhanced intergrain (transport) critical current in the  $\text{YBa}_2\text{Cu}_3\text{O}_{7-\delta}/\text{Ag}$  (10 wt. %) ceramic composite.

## II. EXPERIMENTAL PROCEDURE

### A. Sample preparation

The measurements were performed on disk-shaped samples of the pure  $\text{YBa}_2\text{Cu}_3\text{O}_{7-\delta}$  and the  $\text{YBa}_2\text{Cu}_3\text{O}_{7-\delta}/\text{Ag}$  composites. The  $\text{YBa}_2\text{Cu}_3\text{O}_{7-\delta}/\text{Ag}$

composites were prepared by mixing pure  $\text{YBa}_2\text{Cu}_3\text{O}_{7-\delta}$  powder with fine silver metal powder (mean grain size  $\approx 1$   $\mu\text{m}$ ). The  $\text{YBa}_2\text{Cu}_3\text{O}_{7-\delta}$  compound was prepared by the solid-state reaction method from  $\text{Y}_2\text{O}_3$  (99.99% purity),  $\text{CuO}$  (99.999% purity), and  $\text{BaCO}_3$  (99.995% purity). The powder was mixed, ground, formed into a pellet, and reacted at 905 °C for 24 h. The product obtained was re-crushed, reground, mixed with the silver powder (10 wt. % or 30 wt. %), formed into disk-shaped samples (15-mm diameter, 2.5-mm thick) under pressure of 7000 bars, and sintered in flowing oxygen at 925 °C for 7 h. The disks were furnace cooled at the following rates: 6.5 °C/min (900 °C), 3 °C/min (700 °C), and 1.5 °C/min (500 °C).

### B. Experimental techniques

The presence of silver and the grain structure were analyzed by SEM. The grain and the twin boundary network were viewed in a Hitachi H-7000 electron microscope (125 kV). The lattice constants were analyzed using an x-ray powder diffraction pattern recorded by a Rigaku diffractometer ( $\text{CuK}\alpha$  radiation).

The dependence of resistivity on temperature (80–300 K) and superconducting transition temperature at zero resistance were measured using a conventional four-probe technique and a computer-controlled system with a digital nanovoltmeter. Rectangular bar-shaped samples of dimensions  $\sim 11.0 \times 3.0 \times 2.5$   $\text{mm}^3$  with silver-print contacts were used. The temperature was determined by a calibrated Pt thermometer with a calibration accuracy of  $\pm 20$  mK. The temperature was raised or lowered at a rate of about 5 K/h, and at a lower rate near the transition.

The dc magnetization measurements as a function of temperature (10–90 K) and an applied magnetic field (0–30 kG) were made in a Quantum Design SQUID (superconductive quantum interference device) magnetometer. The magnetic hysteresis loops were measured at low magnetic field, up to 200 G and at high fields, up to 45 kG, at 10 and 77 K for zero-field-cooled samples. The "magnetic" critical current densities were determined from the high-field (45 kG) hysteresis loops. As was pointed out by Stollman *et al.*<sup>23</sup> great care should be taken in measuring high-magnetic-field hysteresis loops in the Quantum Design system. The measuring technique in this system is to scan the sample through an array of detection loops and measure the SQUID-voltage output as a function of position with respect to these loops. A scan length should not be larger than the region of constant magnetic field in a solenoid. According to the data provided by Stollman *et al.* we chose the optimum magnitude of a scan length of 6 cm. The magnetic moment was calculated in units emu/g taking into account only the amount of superconducting  $\text{YBa}_2\text{Cu}_3\text{O}_{7-\delta}$  compound (subtracting the weight of silver) in the sample. The diamagnetic moment of silver is about 4–5 orders of magnitude smaller than that of pure  $\text{YBa}_2\text{Cu}_3\text{O}_7$ . The remanent magnetic moment was measured at 12 different temperatures over the range 10–95 K. Before the mea-

surement at each temperature the sample was warmed up to 200 K and then field cooled (at 100 G and 1 kG).

The measurements of the distribution of magnetic field, magnetic flux expulsion, penetration, and pinning, and their dependence on time (the time scale of  $10^4$ – $10^5$  s) and on an applied magnetic field (0–1200 G) were performed at 77 K with an axial cryogenic Hall probe (sensitivity  $\pm 0.030$  G). The probe was scanned along the diameter of a disk-shaped sample and measured the component of magnetic field perpendicular to the sample at a distance of about 1 mm from the sample surface. The probe was connected to a gaussmeter and a computer-controlled system, that also allowed measurements of fast time decays of magnetic flux. A solenoid was used to generate magnetic fields in a direction perpendicular to the disk plane. The disk-shaped pure  $\text{YBa}_2\text{Cu}_3\text{O}_{7-\delta}$  and the  $\text{YBa}_2\text{Cu}_3\text{O}_{7-\delta}/\text{Ag}$  composite samples were all of the same dimensions (15-mm diameter, 2.5-mm thick).

The transport critical current densities were determined at 77 K and  $H=0$  from the current-voltage curves measured using a dc four-probe technique. The voltage drop across the sample was measured by a digital nanovoltmeter. (A signal of  $1 \mu\text{V}$  was used as the indication of reaching the critical current value.) These measurements were performed on rectangular bar-shaped samples. Two sets of bars were prepared, the first of dimensions approximately  $11.0 \times (3.0-2.0) \times 2.5 \text{ mm}^3$  with a neck of cross section approximately  $(3.0-2.0) \times 1.5 \text{ mm}^2$  in the middle, the second of dimensions  $\sim 11.0 \times (3.0-2.5) \times 1.0 \text{ mm}^3$  without a neck. The contacts area of the first set was  $\sim 8.0 \text{ mm}^2$ , and of the second one was  $\sim 2.8 \text{ mm}^2$ . Silver print was used to make the contacts.

### III. EXPERIMENTAL RESULTS

#### A. Scanning electron microscopy, electron microprobe, and transmission electron microscopy analysis

SEM was utilized to study the grain structure of the pure  $\text{YBa}_2\text{Cu}_3\text{O}_{7-\delta}$  and the  $\text{YBa}_2\text{Cu}_3\text{O}_{7-\delta}/\text{Ag}$  (10 and 30 wt. %) composites. Micrographs are displayed in Fig. 1. The pure  $\text{YBa}_2\text{Cu}_3\text{O}_{7-\delta}$  exhibits a broad distribution of grain sizes [Fig. 1(a)]. Silver added to  $\text{YBa}_2\text{Cu}_3\text{O}_7$  makes this distribution more uniform. The average grain size for both 10 and 30 wt. % Ag is about  $6.0$ – $6.5 \mu\text{m}$  [Figs. 1(b) and 1(c)], which is larger than the mean grain size of the pure  $\text{YBa}_2\text{Cu}_3\text{O}_{7-\delta}$  equal to about  $3.5$ – $4.5 \mu\text{m}$ . The distribution of silver in the samples was characterized by an electron microprobe. The x-ray micrographs of fractured surfaces of the  $\text{YBa}_2\text{Cu}_3\text{O}_{7-\delta}/\text{Ag}$  composites (Fig. 2) show silver residing between grains of the  $\text{YBa}_2\text{Cu}_3\text{O}_{7-\delta}$  matrix. Twin boundaries inside grains of the pure  $\text{YBa}_2\text{Cu}_3\text{O}_{7-\delta}$  and the  $\text{YBa}_2\text{Cu}_3\text{O}_{7-\delta}/\text{Ag}$  composites were analyzed in a transmission electron microscope. Figures 3(a)–3(d) present bright-field images of twin boundaries viewed along the direction close to  $[001]$ . It was found by comparing the bright-field images with selected area diffraction patterns that the twinning occurs on the (110) planes. The images show that the size of twins and the spacing between them change over the range 10–100 nm within a single grain. We could not

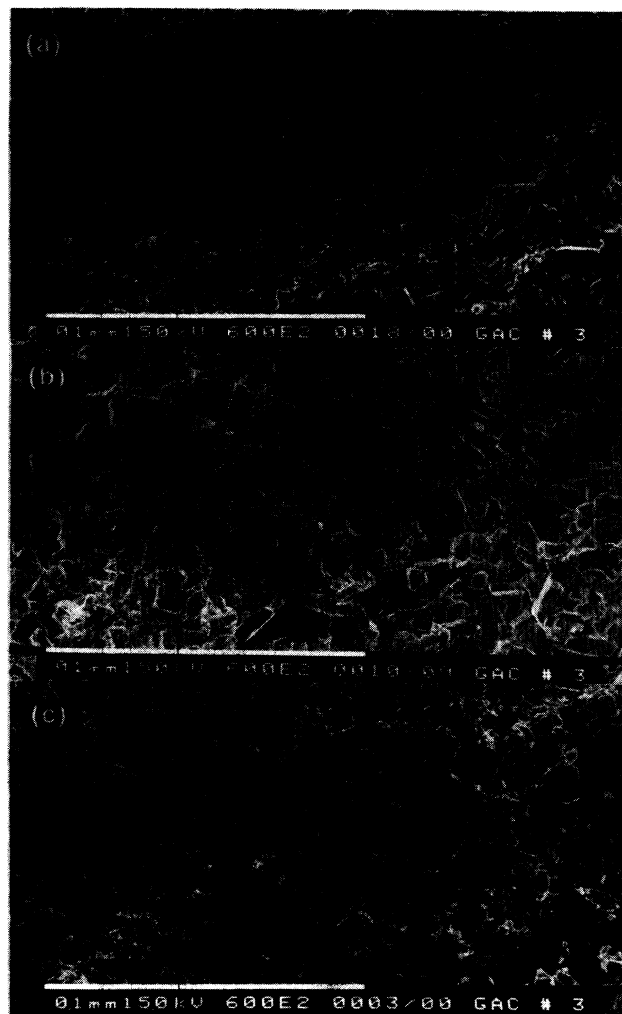


FIG. 1. SEM micrographs showing the grain structure of superconducting ceramics. (a) The pure  $\text{YBa}_2\text{Cu}_3\text{O}_{7-\delta}$  sample, showing the broad distribution of grain sizes; the average grain size is  $3.7 \mu\text{m}$ . (b) The  $\text{YBa}_2\text{Cu}_3\text{O}_{7-\delta}/\text{Ag}$  (10 wt. %) composite showing the uniform distribution of grain sizes; the average grain size is  $6.1 \mu\text{m}$ . (c) The  $\text{YBa}_2\text{Cu}_3\text{O}_{7-\delta}/\text{Ag}$  (30 wt. %) composite. The average grain size is  $6.4 \mu\text{m}$ .

find a change in a number of twins, and in the twin size and spacing between different grains and between the pure  $\text{YBa}_2\text{Cu}_3\text{O}_{7-\delta}$  and the  $\text{YBa}_2\text{Cu}_3\text{O}_{7-\delta}/\text{Ag}$  composites.

#### B. X-ray powder-diffraction analysis

The x-ray diffraction patterns taken for the powder of the pure  $\text{YBa}_2\text{Cu}_3\text{O}_{7-\delta}$  and the  $\text{YBa}_2\text{Cu}_3\text{O}_{7-\delta}/\text{Ag}$  composites are shown in Fig. 4 for angles  $2\theta(\text{CuK}\alpha)$  over the range  $10^\circ$ – $90^\circ$ . For the  $\text{YBa}_2\text{Cu}_3\text{O}_{7-\delta}/\text{Ag}$  composites one can see the presence of the (111), (200), and (220) reflections of Ag in the x-ray diffraction patterns. The ratio of intensities of the x-ray reflections changes in the  $\text{YBa}_2\text{Cu}_3\text{O}_{7-\delta}/\text{Ag}$  composites, e.g., the ratio of the inten-

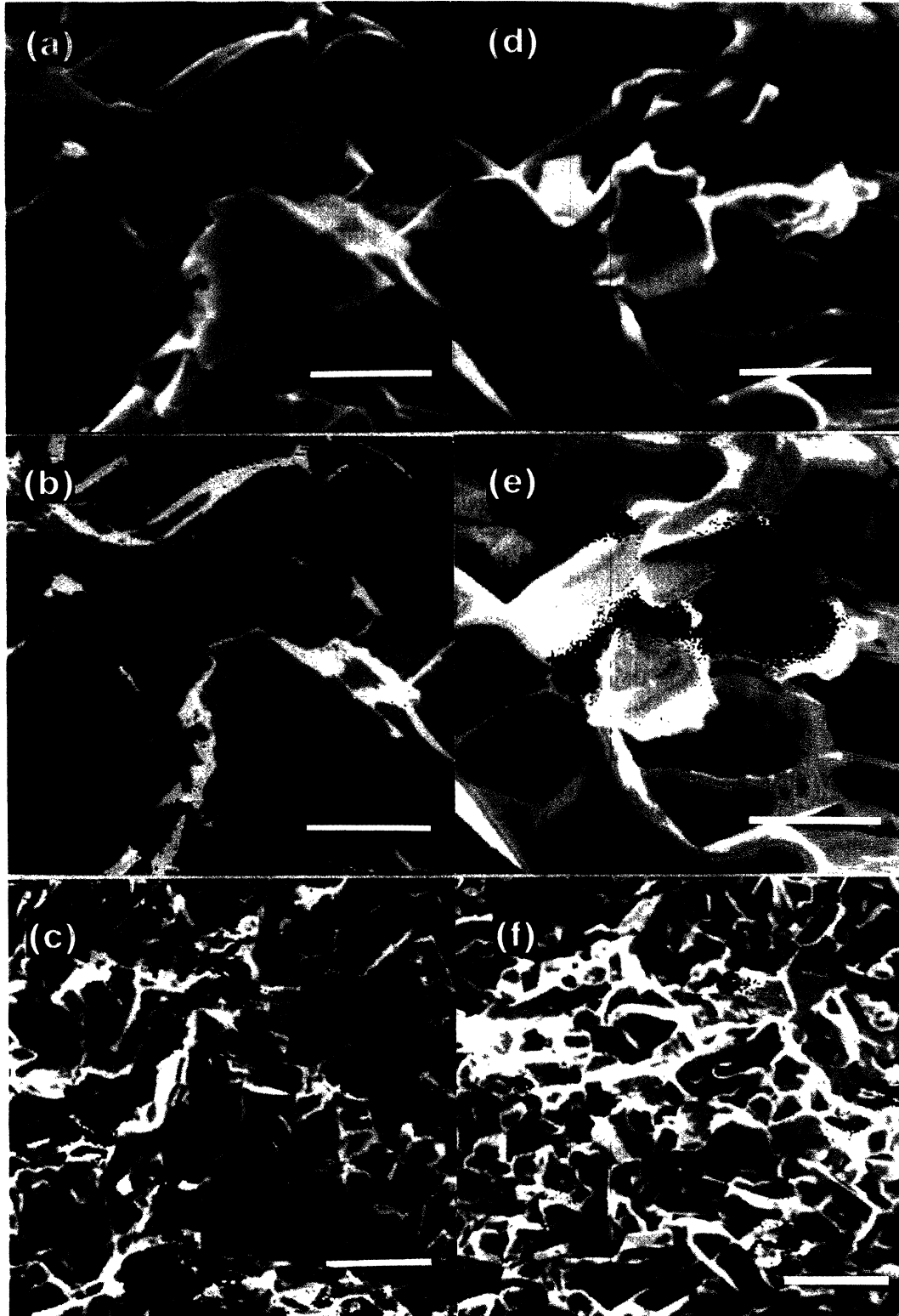


FIG. 2. SEM and electron microprobe micrographs of fractured surfaces of the  $\text{YBa}_2\text{Cu}_3\text{O}_{7-\delta}/\text{Ag}$  composites. It can be seen that silver resides between the  $\text{YBa}_2\text{Cu}_3\text{O}_{7-\delta}$  grains; (a), (b), and (c) the  $\text{YBa}_2\text{Cu}_3\text{O}_{7-\delta}/\text{Ag}$  (30 wt. %) composite; (d), (e), and (f) the  $\text{YBa}_2\text{Cu}_3\text{O}_{7-\delta}/\text{Ag}$  (10 wt. %) composite; (a) and (d) the SEM micrographs of grains; (b), (c), (e), and (f) the x-ray micrographs of silver (red) filling intergranular space. The scale bars on (a), (b), (d), and (e) mark  $5\mu\text{m}$ . The scale bars on (c) and (f) mark  $20\mu\text{m}$ .

sity of the (103), (110) reflection and the intensity of the (013) reflection decreases of silver is added to  $\text{YBa}_2\text{Cu}_3\text{O}_{7-\delta}$ . The lattice parameters of the pure  $\text{YBa}_2\text{Cu}_3\text{O}_{7-\delta}$  and the  $\text{YBa}_2\text{Cu}_3\text{O}_{7-\delta}/\text{Ag}$  composites were calculated using the (006), (020), and (200) reflections (Table I). The lattice parameters  $c$  and  $a$  of the  $\text{YBa}_2\text{Cu}_3\text{O}_{7-\delta}/\text{Ag}$ (30 wt.%) composite are larger than corresponding ones of the pure  $\text{YBa}_2\text{Cu}_3\text{O}_{7-\delta}$  and the  $\text{YBa}_2\text{Cu}_3\text{O}_{7-\delta}/\text{Ag}$ (10 wt.%) composite. No changes of the lattice constant  $b$  were observed.

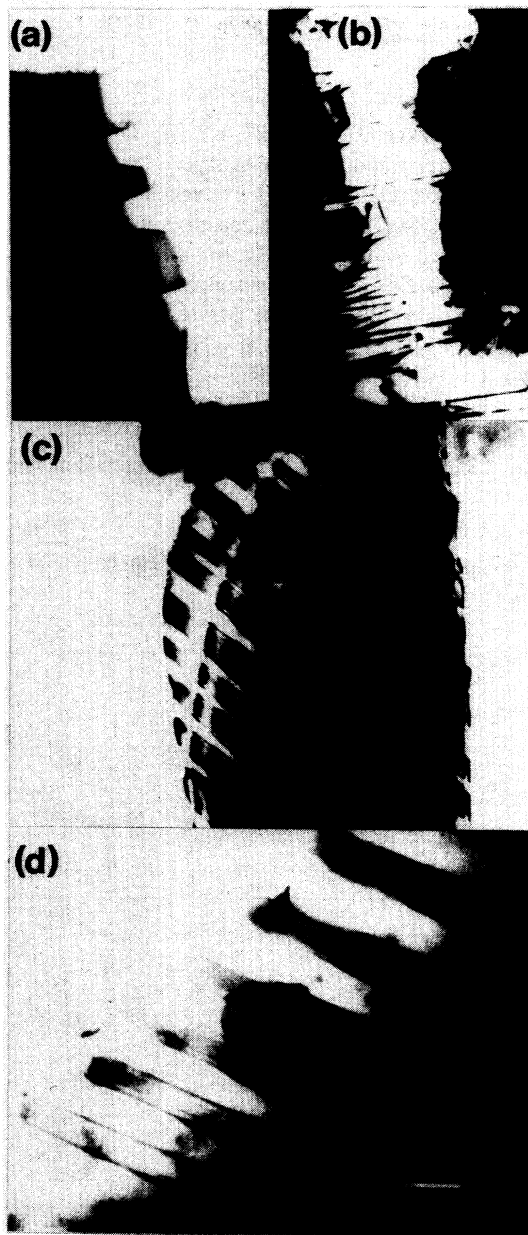


FIG. 3. TEM bright-field images of twin boundaries of the pure  $\text{YBa}_2\text{Cu}_3\text{O}_{7-\delta}$  and the  $\text{YBa}_2\text{Cu}_3\text{O}_{7-\delta}/\text{Ag}$  composites viewed along the direction close to [001]. Twinning occurs on the (110) planes. (a) and (b) Twins in the pure  $\text{YBa}_2\text{Cu}_3\text{O}_{7-\delta}$  grains; (c) twins in the  $\text{YBa}_2\text{Cu}_3\text{O}_{7-\delta}/\text{Ag}$ (10 wt.%) composite; (d) twins in the  $\text{YBa}_2\text{Cu}_3\text{O}_{7-\delta}/\text{Ag}$ (30 wt.%) composite. The scale bar marks 100 nm.

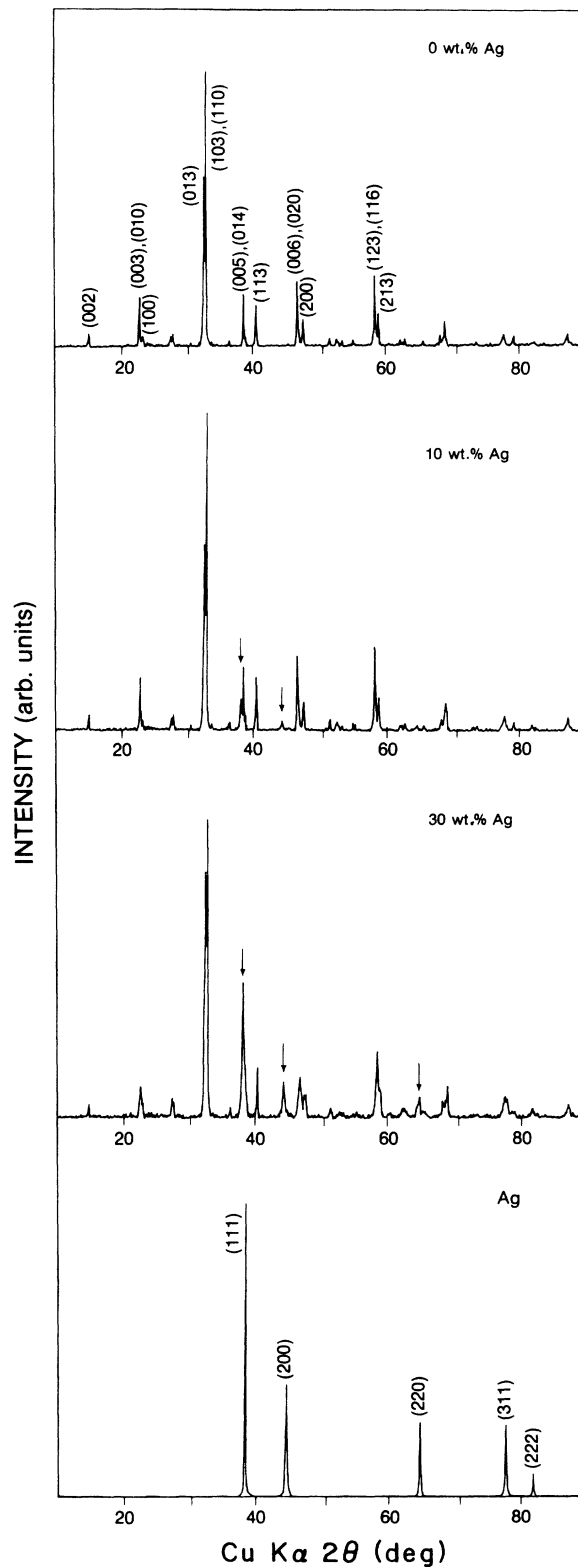


FIG. 4. The x-ray diffraction patterns taken for the powder of the pure  $\text{YBa}_2\text{Cu}_3\text{O}_{7-\delta}$ , the  $\text{YBa}_2\text{Cu}_3\text{O}_{7-\delta}/\text{Ag}$  composites, and pure silver. The arrows indicate the reflections of pure silver.

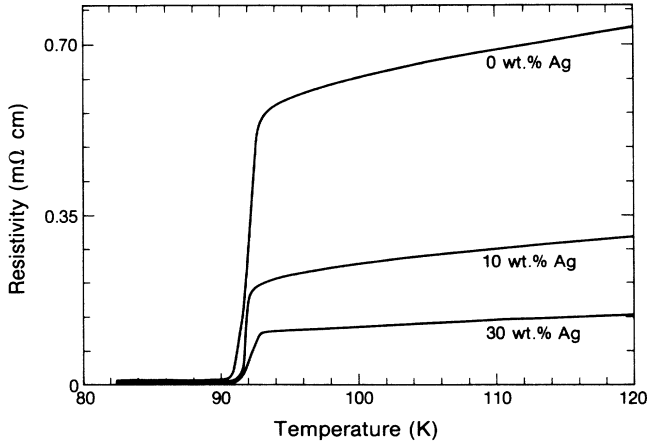


FIG. 5. Resistivity vs temperature, measured for the pure  $\text{YBa}_2\text{Cu}_3\text{O}_{7-\delta}$  sample (the upper curve) and the  $\text{YBa}_2\text{Cu}_3\text{O}_{7-\delta}/\text{Ag}$  composites. The normal-state resistivity is being reduced by the presence of silver. For the  $\text{YBa}_2\text{Cu}_3\text{O}_{7-\delta}/\text{Ag}$  composites  $T_c^{R=0}$  is slightly higher (91.0 K) than that for the pure  $\text{YBa}_2\text{Cu}_3\text{O}_{7-\delta}$  sample (90.5 K).

### C. Resistivity, magnetic susceptibility, and remanent moment measurements

Resistivity measurements were performed for three samples: the pure  $\text{YBa}_2\text{Cu}_3\text{O}_{7-\delta}$  and the

TABLE I. Lattice parameters and oxygen content in the pure  $\text{YBa}_2\text{Cu}_3\text{O}_{7-\delta}$  and the  $\text{YBa}_2\text{Cu}_3\text{O}_{7-\delta}/\text{Ag}$  composites. The calculation of lattice parameters is based on the analysis of the reflections (006), (020), and (200). The calculation of oxygen content is based on the relationship between lattice parameter  $c$  and  $\delta$  equal to  $dc/d\delta = +0.047 \text{ \AA}$  (Ref. 43). It was assumed that  $c/3 = 3.890 \text{ \AA}$  corresponds to  $\delta = 0$ .

Sample (wt. % Ag)	$a$ ( $\text{\AA}$ )	$b$ ( $\text{\AA}$ )	$c$ ( $\text{\AA}$ )	Oxygen content ( $7-\delta$ )
0	3.818	3.886	11.676	6.957
10	3.818	3.886	11.682	6.915
30	3.826	3.886	11.694	6.830

$\text{YBa}_2\text{Cu}_3\text{O}_{7-\delta}/\text{Ag}$ (10 and 30 wt. %) composites (Fig. 5). The normal-state resistivity at 120 K of the  $\text{YBa}_2\text{Cu}_3\text{O}_{7-\delta}/\text{Ag}$ (30 wt. %) and the  $\text{YBa}_2\text{Cu}_3\text{O}_{7-\delta}/\text{Ag}$ (10 wt. %) composites is reduced by a factor 5 and 2.5, respectively, in comparison with the pure  $\text{YBa}_2\text{Cu}_3\text{O}_{7-\delta}$ . The superconducting transition temperature is slightly higher for the  $\text{YBa}_2\text{Cu}_3\text{O}_{7-\delta}/\text{Ag}$  composites ( $T_c^{R=0} = 91.0 \text{ K}$ ) than for the pure  $\text{YBa}_2\text{Cu}_3\text{O}_{7-\delta}$  ( $T_c^{R=0} = 90.5 \text{ K}$ ).

The magnetic susceptibility of all the samples was measured between 10 and 90 K in magnetic fields of 10 G, 100 G, 1 kG, and 30 kG (Fig. 6). These data were ob-

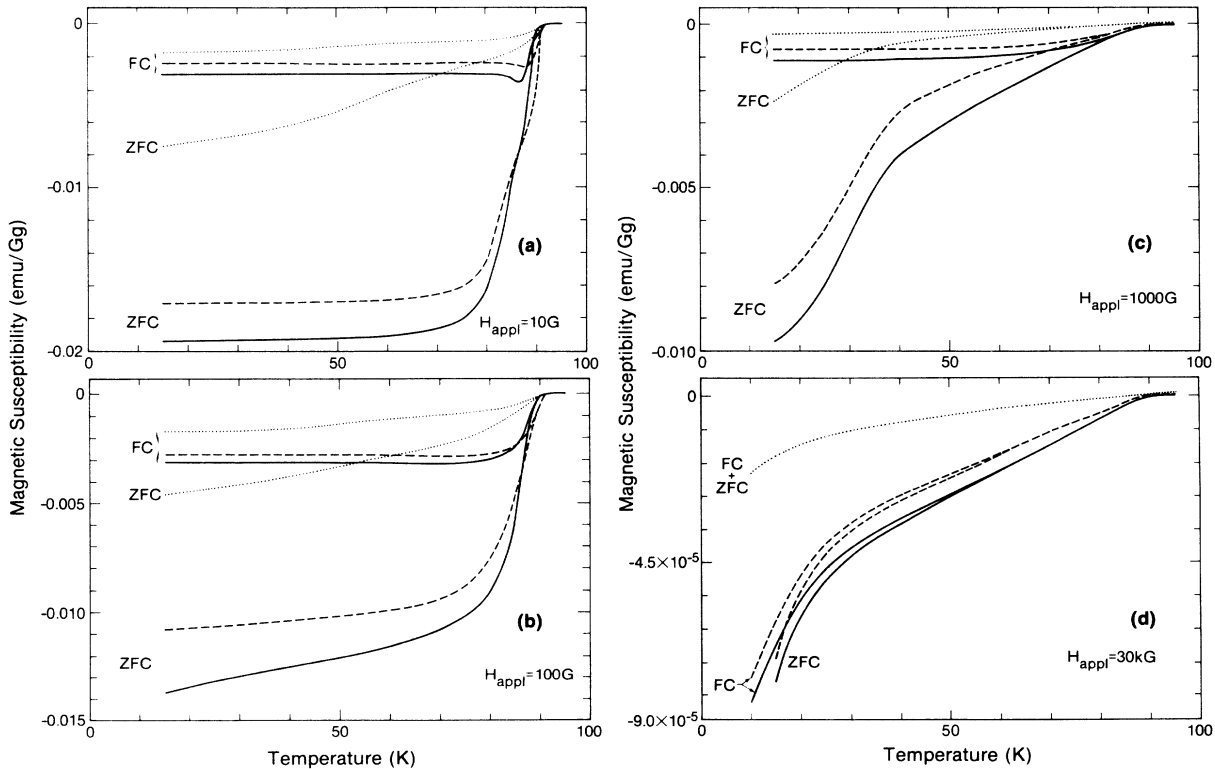


FIG. 6. Magnetic susceptibility vs temperature, measured for the pure  $\text{YBa}_2\text{Cu}_3\text{O}_{7-\delta}$  (solid curve), the  $\text{YBa}_2\text{Cu}_3\text{O}_{7-\delta}/\text{Ag}$ (10 wt. %) composite (dashed curve), and the  $\text{YBa}_2\text{Cu}_3\text{O}_{7-\delta}/\text{Ag}$ (30 wt. %) composite (dotted curve) at different applied magnetic fields: (a) 10 G; (b) 100 G; (c) 1000 G; (d) 30 kG. Both the difference in magnetic moments  $M_{\text{ZFC}} - M_{\text{FC}}$  and the temperature at which reversibility of magnetic moment is observed ( $M_{\text{ZFC}} = M_{\text{FC}}$ ) decrease if silver is added to  $\text{YBa}_2\text{Cu}_3\text{O}_{7-\delta}$ .

tained for both the zero-field-cooling (ZFC) and field-cooling (FC) cases. The magnetic moment  $M = M_{FC} - M_{ZFC}$  where  $M_{FC}, M_{ZFC}$  are field-cooled and zero-field-cooled magnetic moments, respectively, decreases when silver is added to  $YBa_2Cu_3O_{7-\delta}$ . At an applied magnetic field of 1 kG reversibility of the magnetic moment ( $M = 0$ ) occurs above  $\sim 83, 82,$  and  $74$  K for the pure  $YBa_2Cu_3O_{7-\delta}$  and the  $YBa_2Cu_3O_{7-\delta}/Ag(10$  and  $30$  wt. %) composites, respectively [Fig. 6(c)]. At 30 kG a sample of the  $YBa_2Cu_3O_{7-\delta}/Ag(30$  wt. %) composite shows full reversibility over the whole measured range of temperatures down to 10 K. The pure  $YBa_2Cu_3O_{7-\delta}$  and the  $YBa_2Cu_3O_{7-\delta}/Ag(10$  wt. %) composite show reversibility above  $\sim 60$  K [Fig. 6(d)]. The measurements of remanent moment as a function of temperature were made for all samples after field cooling at 100 G and at 1 kG [Figs. 7(a) and 7(b)]. Silver present in  $YBa_2Cu_3O_{7-\delta}$  reduces the remanent moment for field cooling both at 100 G and 1 kG.

#### D. The distributions of magnetic field across the sample, the shielding, the Meissner effect, and the trapped field

Measurements of the distribution of magnetic field, the dependence of flux expulsion, penetration and pinning on

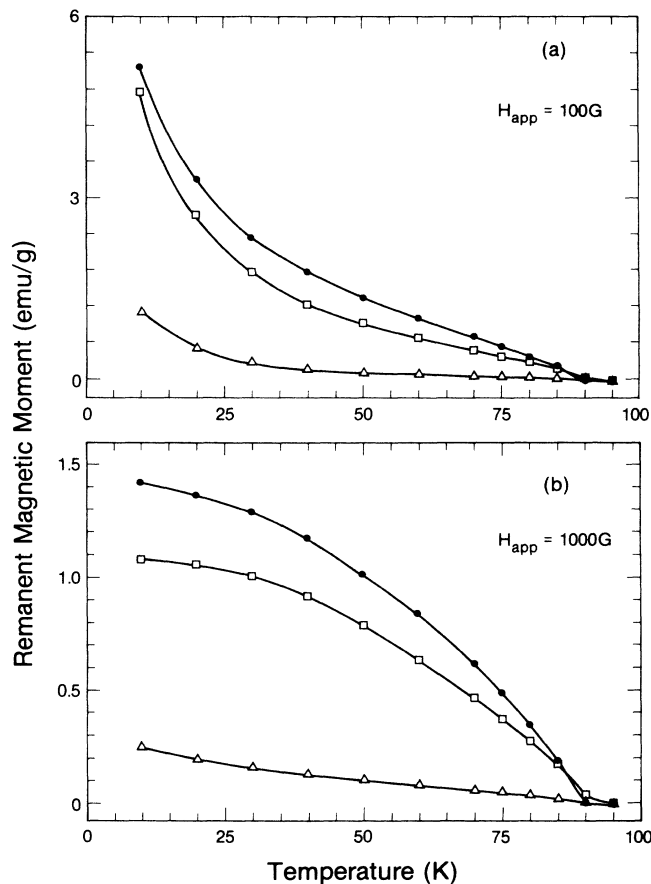


FIG. 7. Remanent magnetic moment vs temperature, measured for the  $YBa_2Cu_3O_{7-\delta}$  (●), the  $YBa_2Cu_3O_{7-\delta}/Ag(10$  wt. %) composite (□), and the  $YBa_2Cu_3O_{7-\delta}/Ag(30$  wt. %) composite (△). Each point on these curves was measured at zero field after field cooling at 100 G (a) or 1 kG (b). The remanent moment decreases if silver is added to  $YBa_2Cu_3O_{7-\delta}$ .

an applied magnetic field, and the dependence of the trapped field on time have been performed at 77 K for both zero-field cooling and field cooling. The measurements were done on the pure  $YBa_2Cu_3O_{7-\delta}$  and the  $YBa_2Cu_3O_{7-\delta}/Ag$  composites.

#### 1. $YBa_2Cu_3O_{7-\delta}/Ag(10$ wt. %) composite

a. *Zero-field cooling.* Magnetic field distributions were measured across the disk-shaped sample at different applied magnetic fields. These distributions are qualitatively similar to those for the pure  $YBa_2Cu_3O_{7-\delta}$  disk-shaped sample.<sup>24</sup> However, the penetration of the magnetic field into the pure  $YBa_2Cu_3O_{7-\delta}$  sample is much slower than into the sample of the  $YBa_2Cu_3O_{7-\delta}/Ag$  composite. Figure 8(a) presents the dependence of the diamagnetic shielding field on the applied magnetic field, measured at the center of the disk-shaped sample of  $YBa_2Cu_3O_{7-\delta}/Ag(10$  wt. %) composite. The shielding field has two maxima at an applied field of 15 and 100 G. The shielding of the pure  $YBa_2Cu_3O_{7-\delta}$  (open circles) is stronger and exhibits maxima at higher applied fields of 35 and 160 G. No time-dependent decay of shielding was observed in the pure  $YBa_2Cu_3O_{7-\delta}$  or the

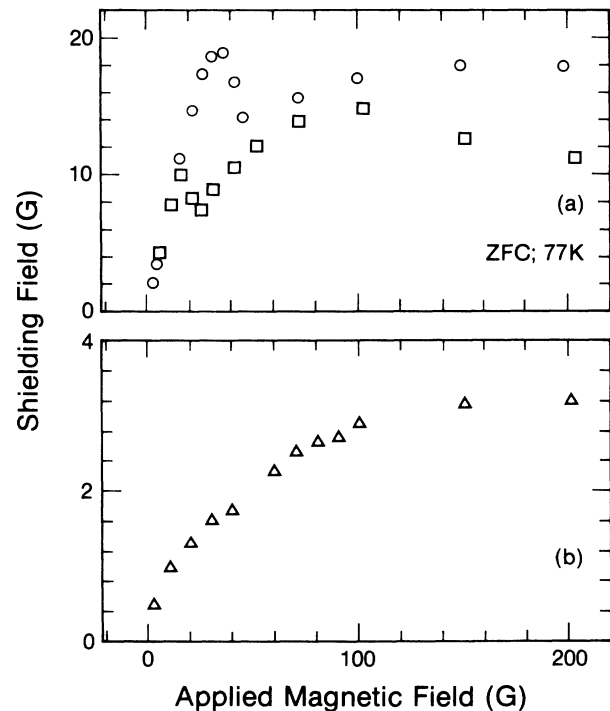


FIG. 8. The dependence of the diamagnetic shielding field on the applied field, measured at 77 K for the zero-field-cooled disks of the  $YBa_2Cu_3O_{7-\delta}/Ag(10$  wt. %) composite, (a), and the  $YBa_2Cu_3O_{7-\delta}/Ag(30$  wt. %) composite, (b), at their centers. The shielding of the 10 wt. % Ag composite exhibits two maxima at 15 and 100 G similar to that of the pure  $YBa_2Cu_3O_{7-\delta}$ . The shielding of the 30 wt. % Ag composite, (b), is weaker than that measured in the 10 wt. % Ag composite, (a), and does not exhibit maxima. The circles show shielding field vs the applied field for the disk of pure  $YBa_2Cu_3O_{7-\delta}$ .

$\text{YBa}_2\text{Cu}_3\text{O}_{7-\delta}/\text{Ag}$  composites within the accuracy of our measurements ( $\pm 0.030$  G). The presence of 10 wt. % of silver in  $\text{YBa}_2\text{Cu}_3\text{O}_{7-\delta}$  reduces the magnitude of the trapped field by a factor of 2 at applied fields above 40 G [see Fig. 9(a)]. The trapped field in this sample reaches saturation at an applied field of 150 G. The trapped field decays logarithmically in time. The logarithmic decay rate is proportional to the magnitude of an initial trapped magnetic field [Fig. 10(a)]. The logarithmic decay rates are higher in the sample of the  $\text{YBa}_2\text{Cu}_3\text{O}_{7-\delta}/\text{Ag}$  composite than those in the pure one. The maximum decay rate corresponds to applied fields above 150 G.

*b. Field cooling.* The distributions of magnetic field were measured across the disk-shaped sample at different applied fields. These distributions are qualitatively similar to those for the pure  $\text{YBa}_2\text{Cu}_3\text{O}_{7-\delta}$  sample.<sup>24</sup> The dependence of the maximum Meissner field (measured at the disk center) on the applied field is shown in Fig. 11(a). At applied fields above 70–100 G the Meissner effect is stronger in the pure  $\text{YBa}_2\text{Cu}_3\text{O}_{7-\delta}$  sample. The magnitude of the trapped field (measured at the disk center) in the  $\text{YBa}_2\text{Cu}_3\text{O}_{7-\delta}/\text{Ag}$  composite is a factor of about 2 smaller than that in the pure  $\text{YBa}_2\text{Cu}_3\text{O}_{7-\delta}$  sample at applied fields above 20 G [see Fig. 12(a)]. The trapped field reaches saturation at an applied field above 50 G. This trapped field decreases logarithmically in time. The loga-

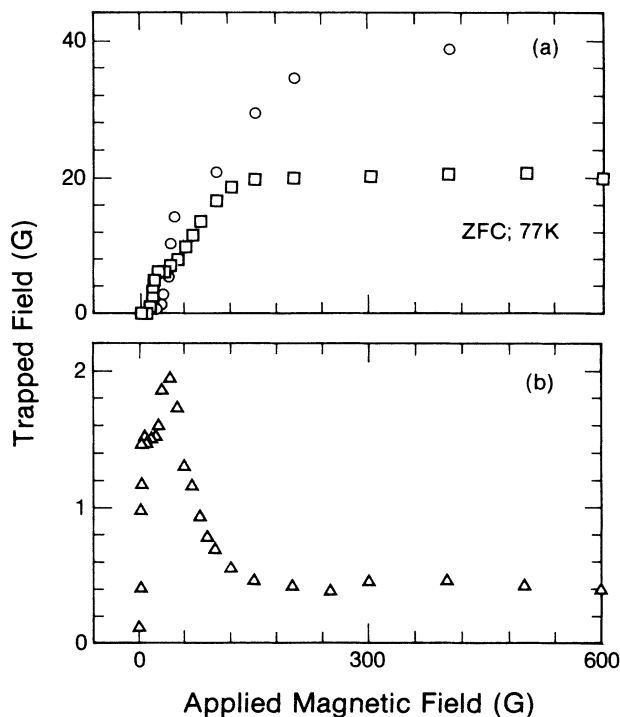


FIG. 9. The dependence of the trapped field measured at 77 K at the center of the zero-field-cooled disks of the  $\text{YBa}_2\text{Cu}_3\text{O}_{7-\delta}/\text{Ag}$ (10 wt. %) composite, (a), and the  $\text{YBa}_2\text{Cu}_3\text{O}_{7-\delta}/\text{Ag}$ (30 wt. %) composite, (b), on the applied field. The circles show the trapped field vs the applied field for the pure  $\text{YBa}_2\text{Cu}_3\text{O}_{7-\delta}$ . The trapped field in the 30 wt. % Ag composite exhibits a maximum of about 2 G at an applied field of about 40 G.

arithmic decay rate is proportional to the initial trapped field [Fig. 13(a)] with a change of a slope at a trapped field of 16 G (corresponding to an applied field around 30 G). The decay rates in the sample of the  $\text{YBa}_2\text{Cu}_3\text{O}_{7-\delta}/\text{Ag}$  composite are higher than those in the pure one as in the ZFC case.

## 2. $\text{YBa}_2\text{Cu}_3\text{O}_{7-\delta}/\text{Ag}$ (30 wt. %) composite

The distributions of the magnetic field measured across the disk-shaped sample are qualitatively similar to those measured in the pure  $\text{YBa}_2\text{Cu}_3\text{O}_{7-\delta}$  and in the  $\text{YBa}_2\text{Cu}_3\text{O}_{7-\delta}/\text{Ag}$ (10 wt. %) composite. However, a large reduction in the diamagnetic shielding, Meissner effect, and trapped field was observed in the

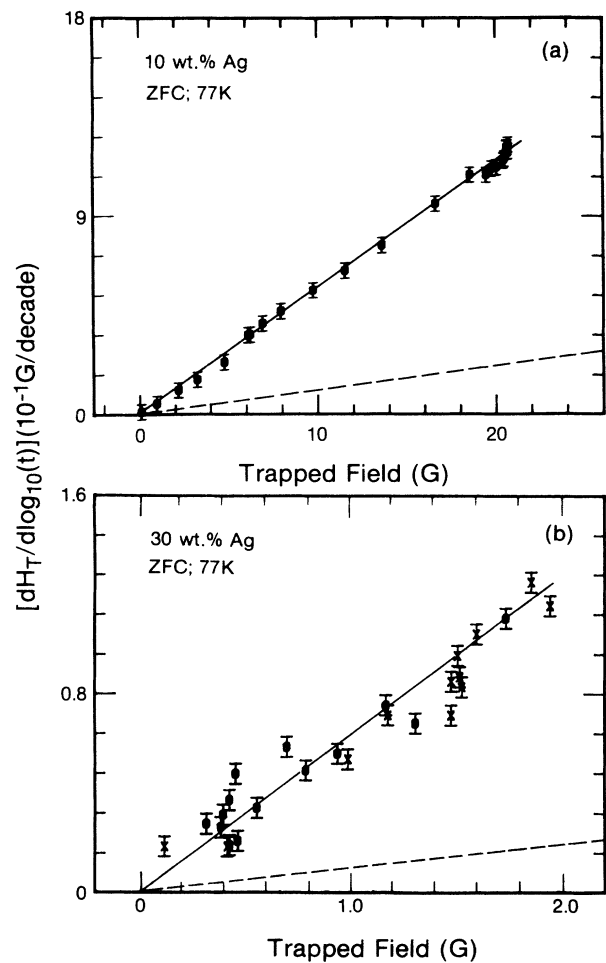


FIG. 10. The dependence of the trapped field decay rate on the initial trapped field, measured at 77 K for the zero-field-cooled disks of the  $\text{YBa}_2\text{Cu}_3\text{O}_{7-\delta}/\text{Ag}$ (10 wt. %) composite, (a), and the  $\text{YBa}_2\text{Cu}_3\text{O}_{7-\delta}/\text{Ag}$ (30 wt. %) composite, (b), at their centers. The slopes give the activation energies for flux creep of 0.28 eV, (a), and 0.26 eV, (b). The symbols ( $\circ$ ) and ( $\times$ ) in (b) mark the decay rate measured at applied fields below and above 40 G, respectively. The dashed lines represent the trapped field decay rate for the disk of the pure  $\text{YBa}_2\text{Cu}_3\text{O}_{7-\delta}$  for both the ZFC and FC cases. It corresponds to the activation energy of  $1.6 \pm 0.3$  eV.

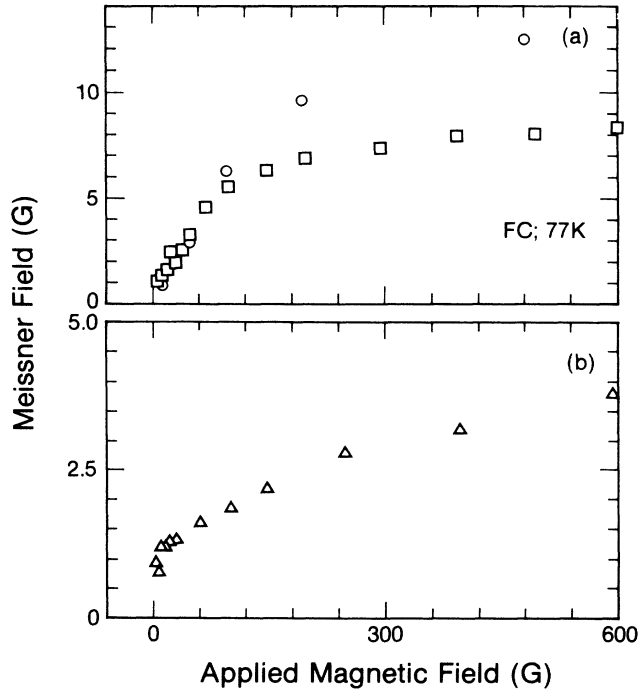


FIG. 11. The Meissner field vs the applied field measured at 77 K for the field-cooled disks of the YBa<sub>2</sub>Cu<sub>3</sub>O<sub>7-δ</sub>/Ag(10 wt.%) composite, (a), and the YBa<sub>2</sub>Cu<sub>3</sub>O<sub>7-δ</sub>/Ag(30 wt.%) composite, (b), at their centers. The circles show the Meissner field measured for the disk of the pure YBa<sub>2</sub>Cu<sub>3</sub>O<sub>7-δ</sub>.

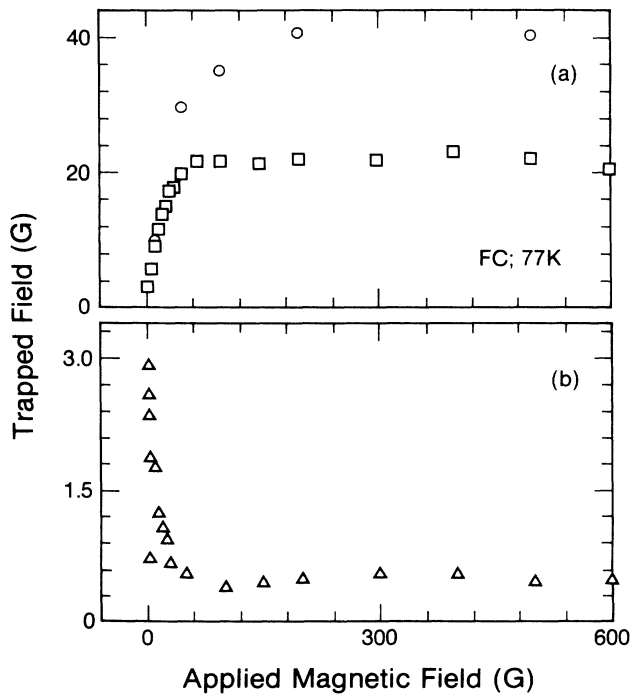


FIG. 12. The trapped field vs the applied field measured at 77 K at the center of the field-cooled disks of the YBa<sub>2</sub>Cu<sub>3</sub>O<sub>7-δ</sub>/Ag(10 wt.%) composite, (a), and the YBa<sub>2</sub>Cu<sub>3</sub>O<sub>7-δ</sub>/Ag(30 wt.%) composite, (b). The trapped field in the 30 wt. % Ag composite exhibits a maximum of about 3 G at an applied field of about 5 G. The circles show the trapped field measured for the pure YBa<sub>2</sub>Cu<sub>3</sub>O<sub>7-δ</sub>.

YBa<sub>2</sub>Cu<sub>3</sub>O<sub>7-δ</sub>/Ag(30 wt. %) composite.

a. *Zero-field cooling.* The dependence of the shielding field on applied magnetic field is shown in Fig. 8(b). The diamagnetic shielding is about three times weaker than that of the YBa<sub>2</sub>Cu<sub>3</sub>O<sub>7-δ</sub>/Ag(10 wt. %) composite. The dependence of the trapped field on applied field is presented in Fig. 9(b). The trapped field exhibits a maximum of 2 G at an applied field of 40 G. This field is a factor of 4 less than the trapped field in the YBa<sub>2</sub>Cu<sub>3</sub>O<sub>7-δ</sub>/Ag(10 wt. %) composite at the same applied field. At an applied field above 100 G the trapped field is reduced down to about 0.5 G, a factor of 40 less

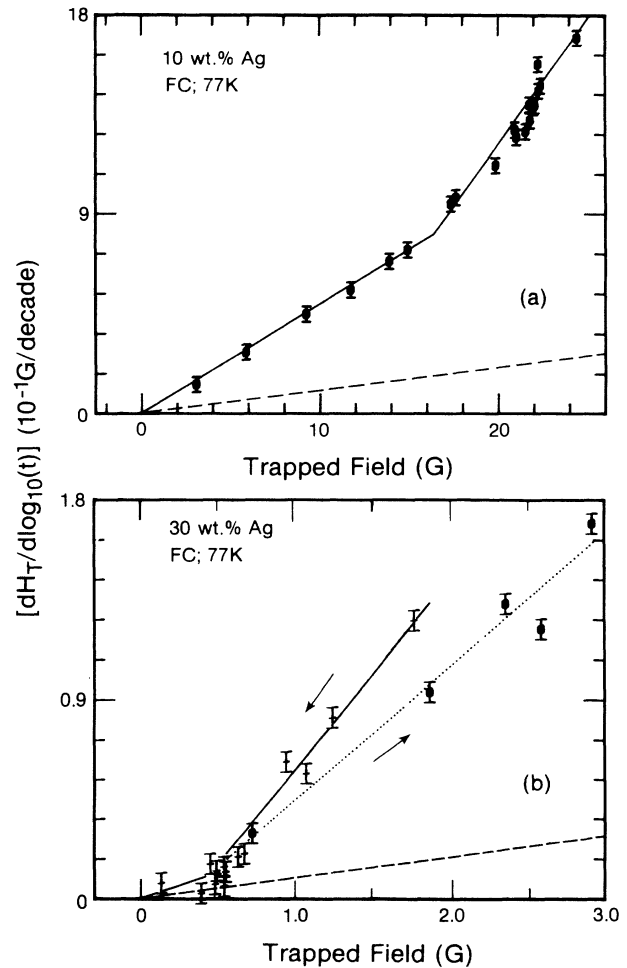


FIG. 13. The dependence of the trapped field decay rate on the initial trapped field measured at 77 K for the field-cooled disks of the YBa<sub>2</sub>Cu<sub>3</sub>O<sub>7-δ</sub>/Ag(10 wt.%) composite, (a), and the YBa<sub>2</sub>Cu<sub>3</sub>O<sub>7-δ</sub>/Ag(30 wt.%) composite, (b), at their centers. For the 10 wt. % Ag composite, (a), the slope gives the activation energy of 0.33 eV for the trapped fields below 16 G (corresponding to applied fields below 40 G) and 0.16 eV for the trapped fields between 16 and 24 G (corresponding to applied fields above 40 G). In (b) (the 30 wt. % Ag composite) the dotted and solid lines show the decay rates measured for applied fields below and above 5 G, respectively. The arrows mark the increasing applied magnetic field. The slopes give the activation energies for flux creep of 0.27 and 0.20 eV, respectively. The dashed lines show the trapped field decay rate measured for the disk of the pure YBa<sub>2</sub>Cu<sub>3</sub>O<sub>7-δ</sub> for both the ZFC and FC cases.

TABLE II. Transport (intergrain) critical current density  $J_{CT}$  and magnetic (intragrain) critical current density  $J_{CM}$  in the pure  $YBa_2Cu_3O_{7-\delta}$  and the  $YBa_2Cu_3O_{7-\delta}/Ag$  composites.

Sample (wt. % Ag)	$T_c$ (K)	Transport $J_{CT}$ ; 77 K (sample with a neck) (A/cm <sup>2</sup> )	Transport $J_{CT}$ ; 77 K (sample without a neck) (A/cm <sup>2</sup> )	Magnetic $J_{CM}$ ; 77 K (A/cm <sup>2</sup> )	Magnetic $J_{CM}$ ; 10 K (A/cm <sup>2</sup> )	Average grain size ( $\mu$ m)
0 <sup>a</sup> No. 1	90.5 ( $R=0$ )	92.2	68.6	$3.64 \times 10^5$		3.7
No. 2	91.2 (magn.)			$4.23 \times 10^5$	$4.73 \times 10^6$	4.5
10	91.0 ( $R=0$ ) 91.4 (magn.)	212.0	230.6	$2.23 \times 10^5$	$3.20 \times 10^6$	6.1
30	91.0 ( $R=0$ ) 91.4 (magn.)	0.15	0.78	$3.77 \times 10^4$	$6.79 \times 10^5$	6.4

<sup>a</sup>The measurement of  $J_{CM}$  was done on two pure  $YBa_2Cu_3O_{7-\delta}$  samples; No. 1 and No. 2.

than the trapped field measured in the 10 wt. % composite. The trapped field decays logarithmically in time. The logarithmic decay rate is proportional to an initial trapped field [Fig. 10(b)]. The decay rates are higher than those in the pure  $YBa_2Cu_3O_{7-\delta}$  sample over the same range of initial trapped fields.

*b. Field cooling.* The dependence of the Meissner field on the applied field is shown in Fig. 11(b). The Meissner field is about two times smaller than that observed in the  $YBa_2Cu_3O_{7-\delta}/Ag$  (10 wt. %) composite. The trapped field depends on the applied magnetic field [Fig. 12(b)]. It shows a maximum of about 3 G at an applied field of 5 G. At applied fields larger than 50 G the trapped field decreases down to about 0.5 G, a factor of 40 less than for the 10 wt. % Ag composite. The trapped field decays logarithmically in time. The logarithmic decay rate is proportional to an initial trapped field like in the ZFC case [Fig. 13(b)]. These decay rates are higher than the corresponding ones in the pure  $YBa_2Cu_3O_{7-\delta}$ . The decay rates corresponding to applied fields above 5 G are higher than those for applied fields below 5 G.

### E. Transport critical-current-density measurements

The transport critical current densities measured in the pure  $YBa_2Cu_3O_{7-\delta}$  and the  $YBa_2Cu_3O_{7-\delta}/Ag$  composites at 77 K and  $H \leq 0.5$  G (the Earth magnetic field) are listed in Table II. The measurements were performed on two sets of rectangular bar-shaped samples with a neck or without it as described before. Similar results were obtained in both cases. The critical current density of the  $YBa_2Cu_3O_{7-\delta}/Ag$  (10 wt. %) composite is about a factor of 3 larger than that of the pure  $YBa_2Cu_3O_{7-\delta}$  sample. On the other hand, the critical current density of the  $YBa_2Cu_3O_{7-\delta}/Ag$  (30 wt. %) composite is about  $10^2$ – $10^3$  times smaller than that of the pure  $YBa_2Cu_3O_{7-\delta}$  sample.

### F. Hysteresis loops and magnetic critical current density

Low-field (up to 200 G) and high-field (up to 45 kG) hysteresis loops were measured at 10 and 77 K for the pure  $YBa_2Cu_3O_{7-\delta}$  and the  $YBa_2Cu_3O_{7-\delta}/Ag$  composites. Figures 14 and 15 present the low-field hysteresis loops. The amplitude of the hysteresis loop shrinks as a function of increasing silver content in  $YBa_2Cu_3O_{7-\delta}$ .

The same was observed for high-field hysteresis loops (Figs. 16 and 17). High-field hysteresis loops were used to calculate the critical current density in the grains. According to Senoussi *et al.*<sup>25</sup> the intragrain critical current density  $J_{CM}$  (in A/cm<sup>2</sup>), the radius of the grain  $R$  (in cm), and the magnetization  $M_+(H)$  and  $M_-(H)$  (in emu/cm<sup>3</sup>) on the ascending and the descending branches

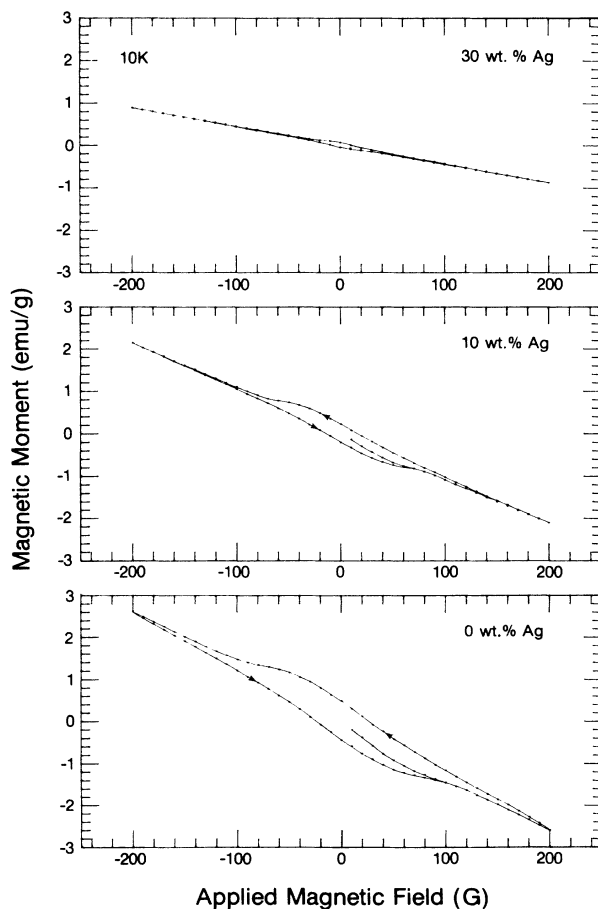


FIG. 14. The low-field (200 G) hysteresis loops measured at 10 K for the pure  $YBa_2Cu_3O_{7-\delta}$  and the  $YBa_2Cu_3O_{7-\delta}/Ag$  composites. Almost reversible behavior is seen for the  $YBa_2Cu_3O_{7-\delta}/Ag$  (30 wt. %) composite.

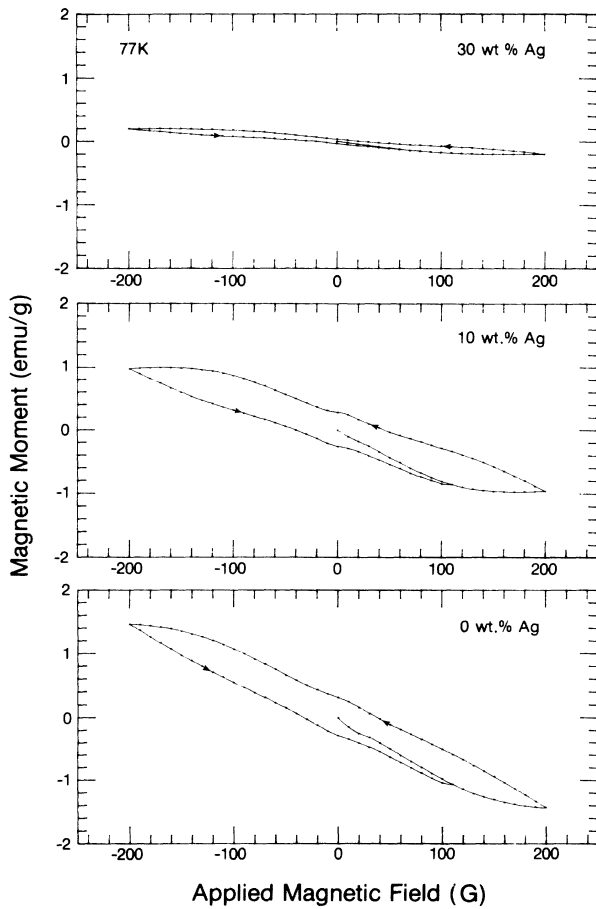


FIG. 15. The low-field (200 G) hysteresis loops measured at 77 K for the pure  $\text{YBa}_2\text{Cu}_3\text{O}_{7-\delta}$  and the  $\text{YBa}_2\text{Cu}_3\text{O}_{7-\delta}/\text{Ag}$  composites.

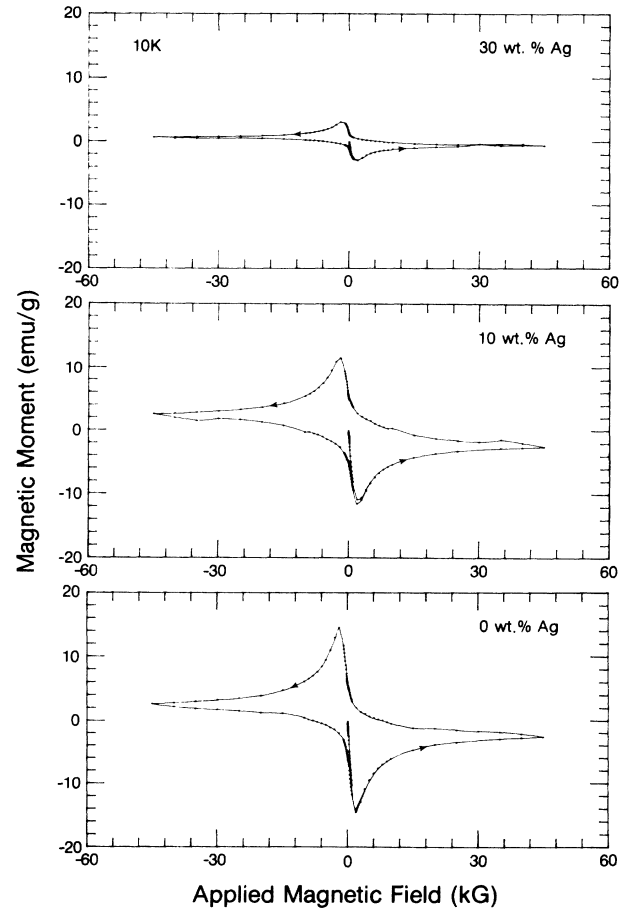


FIG. 16. The high-field (45 kG) hysteresis loops measured at 10 K for the pure  $\text{YBa}_2\text{Cu}_3\text{O}_{7-\delta}$  and the  $\text{YBa}_2\text{Cu}_3\text{O}_{7-\delta}/\text{Ag}$  composites. The loop amplitude shrinks if silver is added to  $\text{YBa}_2\text{Cu}_3\text{O}_{7-\delta}$ .

of the loop, respectively, are related by the formula

$$J_{\text{CM}} = 15[M_+(H) - M_-(H)]/R. \quad (1)$$

The calculated “magnetic” critical current densities within the grains of the pure  $\text{YBa}_2\text{Cu}_3\text{O}_{7-\delta}$  and the  $\text{YBa}_2\text{Cu}_3\text{O}_{7-\delta}/\text{Ag}$  composites at 10 and 77 K are listed in Table II. The intragrain critical current density in the  $\text{YBa}_2\text{Cu}_3\text{O}_{7-\delta}/\text{Ag}$ (10 wt. %) composite at 77 and 10 K is a factor of about 2 smaller than the intragrain current density in the pure  $\text{YBa}_2\text{Cu}_3\text{O}_{7-\delta}$  sample. Correspondingly the critical current density in the  $\text{YBa}_2\text{Cu}_3\text{O}_{7-\delta}/\text{Ag}$ (30 wt. %) composite is about one order of magnitude smaller than that of the  $\text{YBa}_2\text{Cu}_3\text{O}_{7-\delta}$  sample.

#### IV. DISCUSSION

The problem to be discussed is the reason for the enhancement of transport intergrain critical current by intergranular silver present in the  $\text{YBa}_2\text{Cu}_3\text{O}_{7-\delta}$  ceramic superconductor. This effect may be caused either by increased flux pinning in the intergranular regions or by improved coupling between superconducting grains, e.g., via the proximity effect. The coupling between supercon-

ducting grains in the pure  $\text{YBa}_2\text{Cu}_3\text{O}_{7-\delta}$  is believed to occur via arrays of weak links that are either tunnel junctions or point contacts.<sup>26,27</sup> According to the “spin glass” model the weakly coupled grains behave like Josephson junctions.<sup>28,29</sup> Starting at low magnetic fields as the applied field is increased these Josephson junctions are no longer able to sustain the currents necessary for diamagnetic shielding, allowing flux to be trapped in nonsuperconducting regions between the grains. The flux penetrates through the weak-link network in the form of quantized vortices. These vortices are formed by circulating Josephson currents flowing through the weak junctions between grains. Pinning can arise from either discreteness of the Josephson-junction array or inhomogeneity of the junction coupling strengths.<sup>28,29</sup>

The analysis of magnetic properties of the pure  $\text{YBa}_2\text{Cu}_3\text{O}_{7-\delta}$  and the  $\text{YBa}_2\text{Cu}_3\text{O}_{7-\delta}/\text{Ag}$  composites reveals degradation of superconducting properties, i.e., the diamagnetic shielding, Meissner effect, and flux pinning in the  $\text{YBa}_2\text{Cu}_3\text{O}_{7-\delta}/\text{Ag}$  composites. The diamagnetic shielding of the pure  $\text{YBa}_2\text{Cu}_3\text{O}_{7-\delta}$  and the  $\text{YBa}_2\text{Cu}_3\text{O}_{7-\delta}/\text{Ag}$ (10 wt. %) composite exhibits a maximum at an applied magnetic field of 35 and 15 G, respectively [Fig. 8(a)]. However, for the  $\text{YBa}_2\text{Cu}_3\text{O}_{7-\delta}/\text{Ag}$ (30

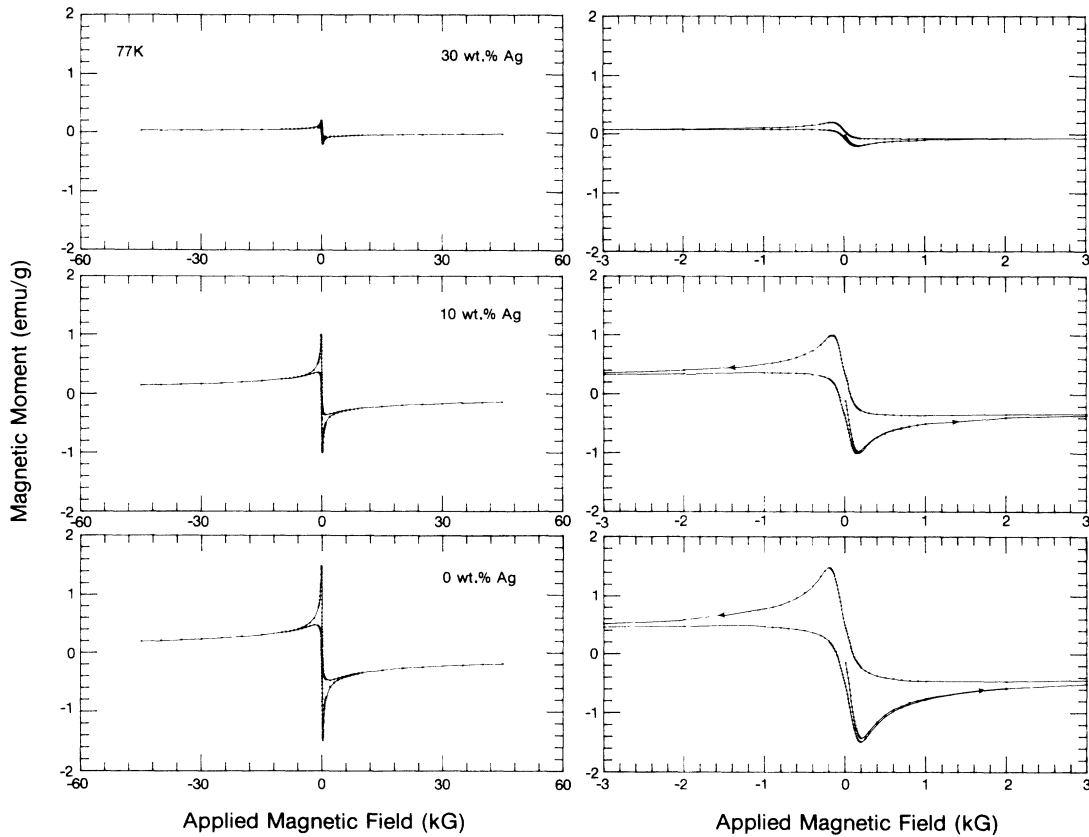


FIG. 17. The high-field (45 kG) hysteresis loops measured at 77 K for the pure  $\text{YBa}_2\text{Cu}_3\text{O}_{7-\delta}$  and the  $\text{YBa}_2\text{Cu}_3\text{O}_{7-\delta}/\text{Ag}$  composites. The figures on the right show the extended region between  $-3$  kG and  $+3$  kG.

wt. %) composite this maximum completely disappears [Fig. 8(b)]. The presence of this maximum indicates that shielding currents flowing through the weak-link junctions between grains reached the critical current value of the intergrain junction. When partial decoupling of grain occurs, e.g., due to silver residing at the grain boundaries, this maximum should be reduced. Partial decoupling is also responsible for the Meissner field being reduced in the  $\text{YBa}_2\text{Cu}_3\text{O}_{7-\delta}/\text{Ag}$  composites. This evidence receives further support from the measurement of the trapped field versus the applied magnetic field in the  $\text{YBa}_2\text{Cu}_3\text{O}_{7-\delta}/\text{Ag}$ (30 wt. %) composite [Figs. 9(b) and 12(b)]. The trapped field has a maximum at low applied fields of 40 and 5 G for the ZFC and FC cases, respectively, while the results for the pure  $\text{YBa}_2\text{Cu}_3\text{O}_{7-\delta}$  and the  $\text{YBa}_2\text{Cu}_3\text{O}_{7-\delta}/\text{Ag}$ (10 wt. %) composite show only saturation for applied fields above 100–150 G. The trapped field is apparently reduced by the addition of silver to  $\text{YBa}_2\text{Cu}_3\text{O}_{7-\delta}$  compound (Figs. 9 and 12).

The activation energy for intergranular flux creep in the pure  $\text{YBa}_2\text{Cu}_3\text{O}_{7-\delta}$  and the  $\text{YBa}_2\text{Cu}_3\text{O}_{7-\delta}/\text{Ag}$  composites was found from the dependence of the logarithmic decay rate of the trapped field  $dH_T(t)/d \ln t$  on the initial trapped field  $H_T(t=0)$  at low applied magnetic fields. According to the theory of flux creep of Hagen, Griessen, and Salomons<sup>30</sup> and Campbell and Evetts<sup>31</sup> in type-II superconductors,  $dH_T/d \ln t$  is proportional to  $H_T(0)$ :

$$\frac{dH_T(t)}{d \ln t} = -H_T(0) \frac{kT}{E}, \quad (2)$$

where  $E = E(H, T)$  is the activation energy for flux creep. The activation energy in the pure  $\text{YBa}_2\text{Cu}_3\text{O}_{7-\delta}$  was found to be  $1.6 \pm 0.3$  eV at 77 K.<sup>32</sup> This is close to a value of 1.55 eV quoted by Maley *et al.*<sup>33</sup> for intergranular flux creep at 75 K and within a range of activation energies calculated by Nikolo and Goldfarb<sup>34</sup> (from  $11.9 \pm 0.3$  eV at an applied field of 0.01 G to  $1.2 \pm 0.3$  eV at 10 G) and Murakami *et al.*<sup>35</sup> (1–3 eV at 1 kG and 77 K). The dependence of  $dH_T(t)/d \ln t = f(H_T(0))$  for the  $\text{YBa}_2\text{Cu}_3\text{O}_{7-\delta}/\text{Ag}$  composites is shown in Figs. 10 and 13 together with that for the pure  $\text{YBa}_2\text{Cu}_3\text{O}_{7-\delta}$ . The activation energy for intergranular flux creep at 77 K in the  $\text{YBa}_2\text{Cu}_3\text{O}_{7-\delta}/\text{Ag}$ (10 wt. %) and  $\text{YBa}_2\text{Cu}_3\text{O}_{7-\delta}/\text{Ag}$ (30 wt. %) composites was found to be within a range 0.26–0.33 eV (see Table III). These energies are in very good agreement with those of 0.30 eV found by Ma *et al.*<sup>22</sup> in the  $\text{YBa}_2\text{Cu}_3\text{O}_{7-\delta}/\text{Ag}$ (5, 15, and 30 wt. %) composites.

The flux trapping at 77 K is being reduced by the intergranular silver by a factor of about 1.3–1.4 in the  $\text{YBa}_2\text{Cu}_3\text{O}_{7-\delta}/\text{Ag}$ (10 wt. %) composite and by a factor of about 10 in the  $\text{YBa}_2\text{Cu}_3\text{O}_{7-\delta}/\text{Ag}$ (30 wt. %) composite as shown by the remanent magnetic moment mea-

sured at low temperatures after field cooling at 100 G and 1 kG, the trapped field measured at 77 K, and the low-field (200 G) hysteresis loops (Figs. 7, 9, 12, 14, and 15). This may indicate that the number of effective pinning centers decreases if silver is added to  $\text{YBa}_2\text{Cu}_3\text{O}_{7-\delta}$ . Grain boundaries in  $\text{YBa}_2\text{Cu}_3\text{O}_{7-\delta}$  are considered to be the pinning centers at low magnetic fields as demonstrated by Wong *et al.*<sup>36</sup> through the measurements of low-field hysteresis loops of ceramics and powders. It is known that during the sintering process intergranular silver wets and cleans grain surfaces and enhances grain growth through partial melting of  $\text{YBa}_2\text{Cu}_3\text{O}_{7-\delta}$ ,<sup>13,16,18</sup> leaving the grains partly coated with a thin layer of metallic silver.<sup>6</sup> One cannot rule out that these chemical processes may change the character of weak links from tunnel junctions [superconductor-insulator-superconductor ( $S/I/S$ )] to normal-metal proximity junctions [superconductor-normal-metal-superconductor ( $S/N/S$ )]. The intergranular coupling energy  $E_J$  is related to the intergranular critical current  $I_c$  (Ref. 29) by

$$E_J = hI_c / 2e. \quad (3)$$

According to Tinkham and Lobb,<sup>29</sup> the coupling energy  $E_J$  and hence critical current  $I_c$  are expected to be less for ( $S/N/S$ )-type junctions than  $S/I/S$  tunnel junctions. They calculated the vortex core energy  $E = 4E_J$  for their cubic array model and concluded that a small amount of randomness in  $E_J$  will suffice for the variations in the local equilibrium vortex energies to provide the pinning. Large variations in the vortex core energies are expected, e.g., from inhomogeneous grain boundaries, difference in tightness of grain contacts, or a range of the  $E_J$  values in the different links. The pinning energy was given as  $U \sim \delta(4E_J)$  and the critical current density was related to  $U$  by

$$J_c = cU / a^2 \phi_0 \quad (4)$$

where  $a$  is the grain size and  $\phi_0 = hc / 2e = 2.07 \times 10^{-7}$  G cm<sup>2</sup> is the superconducting flux quantum.

The proximity junctions between  $\text{YBa}_2\text{Cu}_3\text{O}_{7-\delta}$  and the silver have been studied by Moreland *et al.*,<sup>37</sup> Gijs *et al.*,<sup>38</sup> and Greene *et al.*<sup>39</sup> Moreland *et al.*<sup>37</sup> developed  $S/N/S$  junctions  $\text{YBa}_2\text{Cu}_3\text{O}_{7-\delta}/\text{Ag}/\text{YBa}_2\text{Cu}_3\text{O}_{7-\delta}$  that appeared to be sensitive to the thickness of the deposited Ag layer (5–20 nm). The coherence length of the normal metal at the  $T_c$  of the electrodes was calculated by Likharev<sup>40</sup> to be  $\xi_N(T_c) \approx 100$ –200 nm at  $T_c \approx 4$  K for the noble metals. Taking  $\xi_N(T)$  proportional to  $T^{-1/2}$ ,  $\xi(T_c)$  for  $T_c = 90$  K should be at least 3–4 times smaller ( $20 < \xi < 70$  nm) than that for  $T_c$  of 5–10 K.<sup>37</sup> Strong proximity coupling in  $\text{YBa}_2\text{Cu}_3\text{O}_{7-\delta}/\text{Ag}/\text{Pb}$ , junctions (with a critical current density  $1.7 \times 10^5$  A/cm<sup>2</sup> at 4.0 K) was reported by Gijs *et al.*<sup>38</sup>  $\xi_N(T = 4.2 \text{ K}) = 52$  nm was estimated. The existence of an  $S/N/S$  proximity junction ( $\text{YBa}_2\text{Cu}_3\text{O}_7/\text{Ag}/\text{Pb}$ ) was also proved by Greene *et al.*<sup>39</sup>

Our  $\text{YBa}_2\text{Cu}_3\text{O}_{7-\delta}/\text{Ag}$  composites exhibit a uniform

distribution of sizes of grains (the average grain size 6.0–6.5  $\mu\text{m}$  [Figs. 1(b) and 1(c)]) separated by clean grain boundaries (without the presence of different insulating phases of Y-Ba-Cu-O).<sup>16</sup> This means that inhomogeneities of the intergrain coupling energies and variations of the vortex core energies could be reduced in  $\text{YBa}_2\text{Cu}_3\text{O}_{7-\delta}/\text{Ag}$  composites leading to a pinning energy smaller than that in pure  $\text{YBa}_2\text{Cu}_3\text{O}_{7-\delta}$  ceramics. The comparison of the “transport” critical current densities in the pure  $\text{YBa}_2\text{Cu}_3\text{O}_{7-\delta}$  and the  $\text{YBa}_2\text{Cu}_3\text{O}_{7-\delta}/\text{Ag}$  composites (Table II) with the calculated activation energies (Table III) for intergranular flux creep [ $1.6 \pm 0.3$  eV for the pure  $\text{YBa}_2\text{Cu}_3\text{O}_{7-\delta}$  and 0.26–0.33 eV for the composites  $\text{YBa}_2\text{Cu}_3\text{O}_{7-\delta}/\text{Ag}$ (10 wt. %) and  $\text{YBa}_2\text{Cu}_3\text{O}_{7-\delta}/\text{Ag}$ (30 wt. %)] and the trapped field (Figs. 7, 9, and 12) indicates that intergranular flux pinning is not responsible for changes of the intergranular critical current densities measured in the  $\text{YBa}_2\text{Cu}_3\text{O}_{7-\delta}/\text{Ag}$  composites. Therefore, we suggest that silver added to  $\text{YBa}_2\text{Cu}_3\text{O}_{7-\delta}$  replaces Josephson tunnel junctions ( $S/I/S$ ) with a large number of normal-metal proximity junctions ( $S/N/S$ ), these junctions together being able to sustain larger critical current density than the tunnel junctions alone. We believe that this is the case of the  $\text{YBa}_2\text{Cu}_3\text{O}_{7-\delta}/\text{Ag}$ (10 wt. %) composite showing an increase of “transport” critical current density up to 210–230 A/cm<sup>2</sup> but a decrease of the activation energy for flux creep down to about 0.3 eV (Table III), and the reduction of a number of pinning centers (trapped flux; Figs. 7, 9, and 12). The measurement of magnetic and transport properties of the  $\text{YBa}_2\text{Cu}_3\text{O}_{7-\delta}/\text{Ag}$ (30 wt. %) composite supports this interpretation. The “transport” critical current density in this compound decreases down to 0.15–0.80 A/cm<sup>2</sup>. A number of pinning centers were dramatically reduced as shown by the remanent moment, the trapped field, and the low-field hysteresis loops (Figs. 7, 9, 12, 14, and 15) but the activation energy for flux creep remained close to 0.3 eV as for the  $\text{YBa}_2\text{Cu}_3\text{O}_{7-\delta}/\text{Ag}$ (10 wt. %) composite. As was pointed out earlier, the reduction of the activation energy of  $1.6 \pm 0.3$  eV for the pure  $\text{YBa}_2\text{Cu}_3\text{O}_{7-\delta}$  sample down to  $\sim 0.3$  eV for the  $\text{YBa}_2\text{Cu}_3\text{O}_{7-\delta}/\text{Ag}$  composites could be associated with silver-induced homogeneity of the junction coupling strengths. In the  $\text{YBa}_2\text{Cu}_3\text{O}_{7-\delta}/\text{Ag}$ (30 wt. %) composite the intergranular layer of silver, of thickness larger than the superconducting coherence length, decouples the superconducting grains and reduces a number of proximity junctions and pinning centers. Good evidence of a partial decoupling of grains is revealed by the dependence of the trapped field on an applied magnetic field [Figs. 9(b) and 12(b)] showing the reduction of the trapped field down to about 0.5 G for applied fields above 50–100 G. The same can be deduced from the low-field (200 G) hysteresis loops showing almost reversible behavior (Figs. 14 and 15). For  $\text{YBa}_2\text{Cu}_3\text{O}_{7-\delta}$  powder the low-field hysteresis loops were shown by Wong *et al.*<sup>36</sup> to be completely reversible.

The high-field (45 kG) hysteresis loops measured at 10 and 77 K probe intragranular properties of the pure  $\text{YBa}_2\text{Cu}_3\text{O}_{7-\delta}$  and the  $\text{YBa}_2\text{Cu}_3\text{O}_{7-\delta}/\text{Ag}$  composites, and they are shown in Figs. 16 and 17. The shapes of

TABLE III. Activation energy  $E$  for intergranular flux creep for zero-field and field-cooling cases at 77 K.

Sample (wt. % Ag)	$E$ (eV)		
	ZFC	FC	
0	1.6±0.3	1.6±0.3	
10	0.28±0.02	0.33±0.02	(For $H_{\text{appl}} < 40$ G)
		0.16±0.05 <sup>a</sup>	(For $H_{\text{appl}} > 40$ G)
30	0.26±0.03	0.27±0.04	(For $H_{\text{appl}} < 5$ G)
		0.20±0.04 <sup>a</sup>	(For $H_{\text{appl}} > 5$ G)

<sup>a</sup>The decrease of the activation energy for flux creep could be caused by interaction between vortices and macroscopic persistent currents circulating around voids or normal regions (Ref. 44).

hysteresis loops are similar to those measured by Evetts and Wade<sup>41</sup> for a conventional type-II superconducting Pb-65 at. % In alloy. The intragrain critical current density can be inferred from the high-field hysteresis loops. The values of “magnetic” intragrain  $J_{\text{CM}}$  at 77 K shown in Table I are  $\sim 10^3$ – $10^5$  times larger than “transport” intergranular critical current density. The ratio  $J_{\text{CM}}/J_{\text{CT}}$  equals  $4$ – $5 \times 10^3$  for the pure  $\text{YBa}_2\text{Cu}_3\text{O}_{7-\delta}$ ,  $1 \times 10^3$  for the  $\text{YBa}_2\text{Cu}_3\text{O}_{7-\delta}/\text{Ag}(10 \text{ wt. \%})$  composite, and  $(5$ – $25) \times 10^4$  for the  $\text{YBa}_2\text{Cu}_3\text{O}_{7-\delta}/\text{Ag}(30 \text{ wt. \%})$  composite. This ratio is the smallest for the 10 wt. % Ag composite indicating the largest area of good intergrain contact.

The intragrain critical current densities  $J_{\text{CM}}$  of the  $\text{YBa}_2\text{Cu}_3\text{O}_{7-\delta}/\text{Ag}(10 \text{ wt. \%})$  and the  $\text{YBa}_2\text{Cu}_3\text{O}_{7-\delta}/\text{Ag}(30 \text{ wt. \%})$  composites are reduced by a factor of 2 and 10, respectively, in comparison with that of the pure  $\text{YBa}_2\text{Cu}_3\text{O}_{7-\delta}$  sample. Note that the average grain size estimated from SEM micrographs may be a source of error in calculation of  $J_{\text{CM}}$  [Eq. (1)]. If the large reduction in  $J_{\text{CM}}$  measured in the 30 wt. % Ag composite is caused by diffusion of silver into  $\text{YBa}_2\text{Cu}_3\text{O}_{7-\delta}$  grains and replacement of Cu by Ag it should be associated with a decrease of superconducting transition temperature (see Fig. 5). The other possibility to be considered is the presence of oxygen-deficient phases of  $\text{YBa}_2\text{Cu}_3\text{O}_{7-\delta}$  inside grains of the  $\text{YBa}_2\text{Cu}_3\text{O}_{7-\delta}/\text{Ag}(30 \text{ wt. \%})$  composite. X-ray powder-diffraction patterns (Fig. 4) show the changes in the intensity ratios for different reflections if silver is added to  $\text{YBa}_2\text{Cu}_3\text{O}_{7-\delta}$ . As Farneth *et al.*<sup>42</sup> pointed out such changes are associated with the reduction of oxygen content in  $\text{YBa}_2\text{Cu}_3\text{O}_{7-\delta}$  grains. Singh *et al.*<sup>4</sup> studied the dependence of oxygen content on the depth below the grain surface in  $\text{YBa}_2\text{Cu}_3\text{O}_{7-\delta}/\text{Ag}$  composites, using x-ray diffraction. They found that the oxygen content decreases rapidly with depth for the  $\text{YBa}_2\text{Cu}_3\text{O}_{7-\delta}/\text{Ag}(40 \text{ wt. \%})$  composite suggesting that  $\text{YBa}_2\text{Cu}_3\text{O}_{7-\delta}/\text{Ag}$  composites containing large amounts of intergranular silver have oxygen-deficient structure below the grain surface. According to studies of the relationship between the lattice parameters and oxygen content in  $\text{YBa}_2\text{Cu}_3\text{O}_{7-\delta}$  done by Nakazawa and Ishikawa,<sup>43</sup> the lattice constant  $c$  increases with  $\delta$  according to the formulas  $dc/d\delta = +0.047 \text{ \AA}$ . The increase of lattice parameters  $c$  and  $a$  in the  $\text{YBa}_2\text{Cu}_3\text{O}_{7-\delta}/\text{Ag}$  composites (Table

I) is therefore associated with increasing oxygen deficiency inside grains of  $\text{YBa}_2\text{Cu}_3\text{O}_{7-\delta}$ . The reduction of intragrain  $J_{\text{CM}}$  in the  $\text{YBa}_2\text{Cu}_3\text{O}_{7-\delta}/\text{Ag}(30 \text{ wt. \%})$  composite (Table II) could be explained by an oxygen-deficient intragrain structure of  $\text{YBa}_2\text{Cu}_3\text{O}_{7-\delta}$ .

## V. CONCLUSIONS

We report on systematic studies of magnetic and transport properties of the pure  $\text{YBa}_2\text{Cu}_3\text{O}_{7-\delta}$  and the  $\text{YBa}_2\text{Cu}_3\text{O}_{7-\delta}/\text{Ag}$  composites. The results show that silver degrades the superconducting properties of  $\text{YBa}_2\text{Cu}_3\text{O}_{7-\delta}$ . It enhances, however, the intergrain critical current density [for the  $\text{YBa}_2\text{Cu}_3\text{O}_{7-\delta}/\text{Ag}(10 \text{ wt. \%})$  composite] because of the presence of  $S/N/S$  proximity junctions that provided a larger area of good contact between grains. Our results did not show any relationship between the intergrain critical current density and the activation energy for intergranular flux creep in the pure  $\text{YBa}_2\text{Cu}_3\text{O}_{7-\delta}$  and the  $\text{YBa}_2\text{Cu}_3\text{O}_{7-\delta}/\text{Ag}$  composites. The activation energy in  $\text{YBa}_2\text{Cu}_3\text{O}_{7-\delta}$  is reduced from about 1.6 eV down to about 0.3 eV by intergranular silver. This energy does not depend on the amount of intergranular silver in  $\text{YBa}_2\text{Cu}_3\text{O}_{7-\delta}$ , suggesting similar character of  $S/N/S$  proximity junctions in all  $\text{YBa}_2\text{Cu}_3\text{O}_{7-\delta}/\text{Ag}$  composites. The number of intergrain pinning centers (trapped intergrain magnetic field) decreases with increasing content of Ag and is not related to the magnitude of intergrain critical current density or activation energy for intergranular flux creep. Large reduction of a number of pinning centers in the  $\text{YBa}_2\text{Cu}_3\text{O}_{7-\delta}/\text{Ag}(30 \text{ wt. \%})$  composite may be caused by a layer of silver of thickness larger than the normal metal coherence length  $\xi_N(T)$  in the  $S/N/S$  proximity junctions leading to decoupling of grains. The reduction of intragrain (magnetic) critical current density in the  $\text{YBa}_2\text{Cu}_3\text{O}_{7-\delta}/\text{Ag}(30 \text{ wt. \%})$  composite is caused by an oxygen-deficient structure below the grain surface as indicated by x-ray analysis. However, the number and character of intragrain twin boundaries is not affected by the presence of silver.

## ACKNOWLEDGMENTS

This work was supported by grants from the Natural Sciences and Engineering Research Council (NSERC) of Canada.

- <sup>1</sup>B. Dwir, M. Affronte, and D. Pavuna, *Appl. Phys. Lett.* **55**, 399 (1989).
- <sup>2</sup>B. Dwir, D. Pavuna, M. Affronte, H. Berger, and J. L. Tholence, *J. Supercond.* (to be published).
- <sup>3</sup>K. Tsuchida, Y. Miura, H. Tsudo, and A. Kato, *J. Less-Common Met.* **146**, 19 (1989).
- <sup>4</sup>J. P. Singh, H. L. Leu, R. B. Poeppel, E. van Voorhees, G. T. Goudey, K. Winsley, and D. Shi, *J. Appl. Phys.* **66**, 3154 (1989).
- <sup>5</sup>N. Imanaka, F. Saito, H. Imai, and G. Adachi, *Jpn. J. Appl. Phys. Pt. 2* **28**, L580 (1989).
- <sup>6</sup>B. R. Weinberger, L. Lynds, D. M. Potrepka, D. B. Snow, C. T. Burila, H. E. Eaton, Jr., R. Cipolli, Z. Tan, and J. I Budnick, *Physica C* (Amsterdam) **161**, 91 (1989).
- <sup>7</sup>M. K. Malik, V. D. Nair, A. R. Biswas, R. V. Raghavan, P. Chaddah, P. K. Mishra, G. Ravikumar, and B. A. Dasanacharya, *Appl. Phys. Lett.* **52**, 1525 (1989).
- <sup>8</sup>M. Majoros, F. Hanic, M. Polak, and M. Kedrova, *Mod. Phys. Lett. B* **3**, 981 (1989).
- <sup>9</sup>S. Sen, I. Chen, C. H. Chen, and D. M. Stefanescu, *Appl. Phys. Lett.* **54**, 766 (1989).
- <sup>10</sup>P. N. Peters, R. C. Sisk, E. W. Urban, C. Y. Huang, and M. K. Wu, *Appl. Phys. Lett.* **52**, 2066 (1988).
- <sup>11</sup>Y. Saito, T. Noji, A. Endo, N. Higuchi, K. Fujimoto, T. Oikawa, A. Hattori, and K. Furuse, *Jpn. J. Appl. Phys. Pt. 2* **26**, L832 (1987).
- <sup>12</sup>J. H. Miller, Jr., S. L. Holder, J. D. Hunn, and G. N. Holder, *Appl. Phys. Lett.* **54**, 2256 (1989).
- <sup>13</sup>G. G. Peterson, B. R. Weinberger, L. Lynds, and H. A. Krasinski, *J. Mater. Res.* **3**, 605 (1988).
- <sup>14</sup>D. Pavuna, H. Berger, M. Affronte, J. Van der Maas, J. J. Caponi, M. Guillot, P. Lejay, and J. L. Tholence, *Solid State Commun.* **68**, 535 (1988).
- <sup>15</sup>R. Prasad, N. C. Coni, A. Mohan, S. K. Khera, K. U. Nair, C. K. Gupta, C. V. Tomy, and S. K. Malik, *Mater. Lett.* **7**, 9 (1988).
- <sup>16</sup>F. Deslandes, B. Raveau, P. Dubots, and D. Legat, *Solid State Commun.* **71**, 407 (1989).
- <sup>17</sup>C. Laubschat, M. Domke, M. Prietsch, T. Mandel, M. Bodenbach, G. Kaindl, H. J. Eickenbusch, R. Schoellhorn, R. Miranda, E. Moran, F. Garcia, and M. A. Alario, *Europhys. Lett.* **6**, 555 (1988).
- <sup>18</sup>T. H. Tiefel, S. Jin, R. C. Sherwood, M. E. Davis, G. W. Kammlott, P. K. Gallagher, D. W. Johnson, Jr., R. A. Fastnacht, and W. W. Rhodes, *Mater. Lett.* **7**, 363 (1989).
- <sup>19</sup>S. Baliga and A. L. Jain, *Appl. Phys. A* **49**, 139 (1989).
- <sup>20</sup>Y. Shapira, C. Y. Huang, E. J. McNiff, Jr., P. N. Peters, B. B. Schwartz, and M. K. Wu, *J. Magn. Magn. Mater.* **78**, 19 (1989).
- <sup>21</sup>S. Jin, R. C. Sherwood, E. M. Gyorgy, T. H. Tiefel, R. B. van Dover, S. Nakahara, L. F. Schneemeyer, R. A. Fastnacht, and M. E. Davis, *Appl. Phys. Lett.* **54**, 584 (1989).
- <sup>22</sup>H. Ma, S. Liang, Q. Feng, Y. Sun, S. Yan, and H. Zhang, *Europhys. Lett.* **10**, 375 (1989).
- <sup>23</sup>G. M. Stollman, B. Dam, J. H. P. M. Emmen, and J. Pankert, *Physica C* (Amsterdam) **161**, 444 (1989).
- <sup>24</sup>M.A.-K. Mohamed, J. Jung, and J. P. Franck, *Phys. Rev. B* **39**, 9614 (1989). (The magnetic fields and the decay rate quoted in this reference are in error. They should be multiplied by a factor of 10.)
- <sup>25</sup>S. Senoussi, M. Oussena, and S. Hadjoudj, *J. Appl. Phys.* **63**, 4176 (1988).
- <sup>26</sup>A. P. Malozemoff, in *Physical Properties of High Temperature Superconductors*, edited by D. M. Ginsberg (World Scientific, Singapore, 1989), p. 73.
- <sup>27</sup>D. P. Hampshire, X. Cai, J. Seuntjens, and D. C. Larbalestier, *Supercond. Sci. Tech.* **1**, 12 (1988).
- <sup>28</sup>J. R. Clem, *Physica C* (Amsterdam) **153-155**, 50 (1988).
- <sup>29</sup>M. Tinkham and C. J. Lobb, *Solid State Phys.* **42**, 91 (1989).
- <sup>30</sup>C. W. Hagen, R. P. Griessen, and E. Salomons, *Physica C* (Amsterdam) **157**, 199 (1989).
- <sup>31</sup>A. M. Campbell and J. E. Evetts, *Adv. Phys.* **21**, 199 (1972).
- <sup>32</sup>M.A.-K. Mohamed, J. Jung, and J. P. Franck, *Phys. Rev. B* **41**, 6466 (1990).
- <sup>33</sup>M. P. Maley, M. E. McHenry, J. O. Willis, and L. J. Campbell, *Physica* (Amsterdam) **C 162-163**, 701 (1989).
- <sup>34</sup>M. Nikolo and R. B. Goldfarb, *Phys. Rev. B* **39**, 6615 (1989).
- <sup>35</sup>M. Murakami, M. Morita, and N. Koyama, *Jpn. J. Appl. Phys.* **28**, L1754 (1989).
- <sup>36</sup>D. Wong, A. K. Stamper, D. D. Stancil, and T. E. Schlesinger, *Appl. Phys. Lett.* **53**, 240 (1988).
- <sup>37</sup>J. Moreland, R. H. Omo, J. A. Beall, and M. Madden, *Appl. Phys. Lett.* **54**, 1477 (1989).
- <sup>38</sup>M. A. M. Gijs, D. Scholten, Th. van Rooy, and R. Ijsselsteijn, *Physica C* (Amsterdam) **162-164**, 1615 (1989).
- <sup>39</sup>L. H. Greene, J. B. Barner, W. L. Feldmann, L. A. Farrow, P. F. Miceli, R. Ramesh, B. J. Wilkens, B. G. Bagley, T. M. Tarascon, J. H. Wernick, M. Giroud, and J. M. Rowell, *Physica C* (Amsterdam) **162-164**, 1069 (1989).
- <sup>40</sup>K. K. Likharev, *Rev. Mod. Phys.* **51**, 101 (1979).
- <sup>41</sup>J. E. Evetts and J. M. A. Wade, *J. Phys. Chem. Solids* **31**, 973 (1970).
- <sup>42</sup>W. E. Farneth, R. K. Bordia, E. M. McCarron III, M. K. Crawford, and R. B. Flippin, *Solid State Commun.* **66**, 953 (1988).
- <sup>43</sup>Y. Nakazawa and M. Ishikawa, *Physica C* (Amsterdam) **158**, 381 (1989).
- <sup>44</sup>M.A.-K. Mohamed, J. Jung, and J. P. Franck, *Phys. Rev. B* **41**, 4286 (1990).

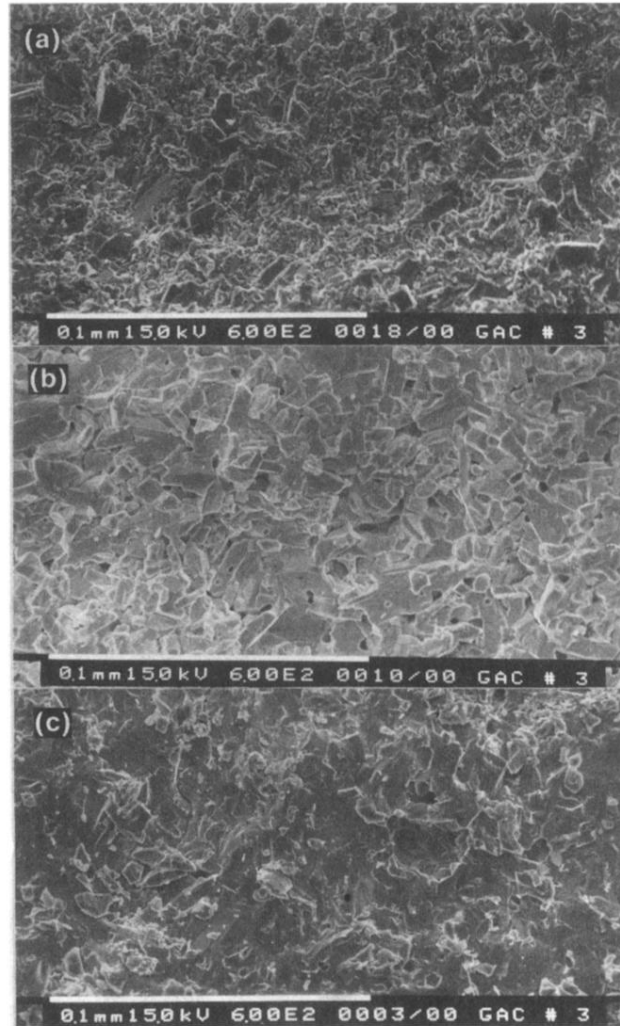


FIG. 1. SEM micrographs showing the grain structure of superconducting ceramics. (a) The pure  $\text{YBa}_2\text{Cu}_3\text{O}_{7-\delta}$  sample, showing the broad distribution of grain sizes; the average grain size is  $3.7 \mu\text{m}$ . (b) The  $\text{YBa}_2\text{Cu}_3\text{O}_{7-\delta}/\text{Ag}(10 \text{ wt. } \%)$  composite showing the uniform distribution of grain sizes; the average grain size is  $6.1 \mu\text{m}$ . (c) The  $\text{YBa}_2\text{Cu}_3\text{O}_{7-\delta}/\text{Ag}(30 \text{ wt. } \%)$  composite. The average grain size is  $6.4 \mu\text{m}$ .

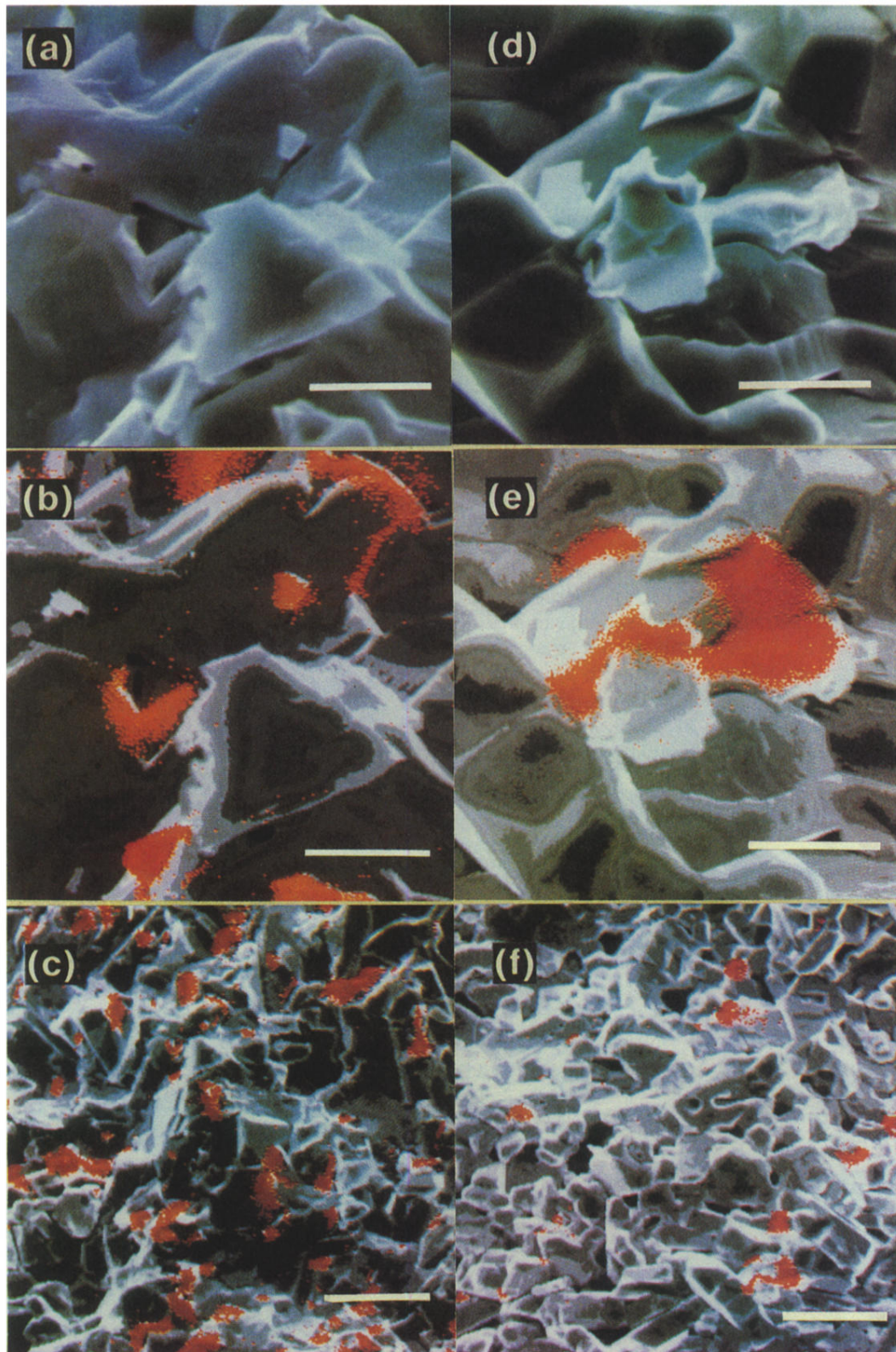


FIG. 2. SEM and electron microprobe micrographs of fractured surfaces of the  $\text{YBa}_2\text{Cu}_3\text{O}_{7-\delta}/\text{Ag}$  composites. It can be seen that silver resides between the  $\text{YBa}_2\text{Cu}_3\text{O}_{7-\delta}$  grains; (a), (b), and (c) the  $\text{YBa}_2\text{Cu}_3\text{O}_{7-\delta}/\text{Ag}$ (30 wt. %) composite; (d), (e), and (f) the  $\text{YBa}_2\text{Cu}_3\text{O}_{7-\delta}/\text{Ag}$ (10 wt. %) composite; (a) and (d) the SEM micrographs of grains; (b), (c), (e), and (f) the x-ray micrographs of silver (red) filling intergranular space. The scale bars on (a), (b), (d), and (e) mark  $5\mu\text{m}$ . The scale bars on (c) and (f) mark  $20\mu\text{m}$ .

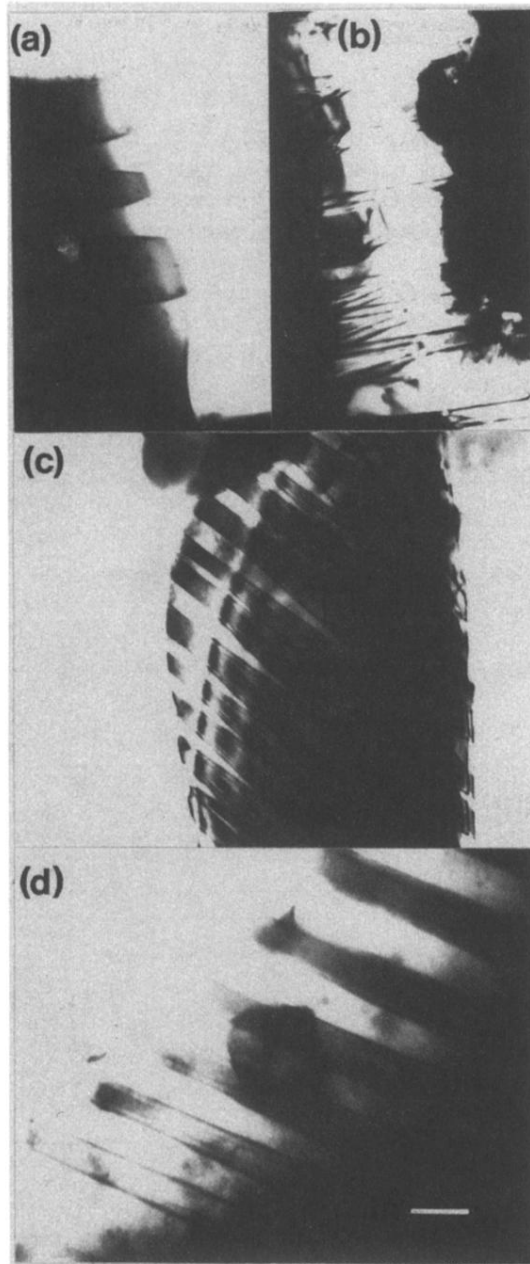


FIG. 3. TEM bright-field images of twin boundaries of the pure  $\text{YBa}_2\text{Cu}_3\text{O}_{7-\delta}$  and the  $\text{YBa}_2\text{Cu}_3\text{O}_{7-\delta}/\text{Ag}$  composites viewed along the direction close to  $[001]$ . Twinning occurs on the  $(110)$  planes. (a) and (b) Twins in the pure  $\text{YBa}_2\text{Cu}_3\text{O}_{7-\delta}$  grains; (c) twins in the  $\text{YBa}_2\text{Cu}_3\text{O}_{7-\delta}/\text{Ag}$ (10 wt. %) composite; (d) twins in the  $\text{YBa}_2\text{Cu}_3\text{O}_{7-\delta}/\text{Ag}$ (30 wt. %) composite. The scale bar marks 100 nm.